

# Image Colorization: A Survey and Dataset

Saeed Anwar\*, Muhammad Tahir\*, Chongyi Li, Ajmal Mian, Fahad Shahbaz Khan, Abdul Wahab Muzaffar

**Abstract**—Image colorization is an essential image processing and computer vision branch to colorize images and videos. Recently, deep learning techniques progressed notably for image colorization. This article presents a comprehensive survey of recent state-of-the-art colorization using deep learning algorithms, describing their fundamental block architectures in terms of skip connections, input *etc.* as well as optimizers, loss functions, training protocols, and training data *etc.* Generally, we can roughly categorize the existing colorization techniques into seven classes. Besides, we also provide some additional essential issues, such as benchmark datasets and evaluation metrics. We also introduce a new dataset specific to colorization and perform an experimental evaluation of the publicly available methods. In the last section, we discuss the limitations, possible solutions, and future research directions of the rapidly evolving topic of deep image colorization that the community should further address. Dataset and Codes for evaluation will be publicly available at <https://github.com/saeed-anwar/ColorSurvey>

**Index Terms**—Image colorization, deep learning, experimental survey, new colorization dataset, colorization review, CNN model classification.



## 1 INTRODUCTION

“Don't ask what love can make or do! Look at the colors of the world.” - Rumi

COLORIZATION of images is a challenging problem due to the varying image conditions that need to be dealt via a single algorithm. The problem is also severely ill-posed as two out of the three image dimensions are lost; although the semantics of the scene may be helpful in many cases, for example, grass is usually green, clouds are usually white, and the sky is blue. However, such semantic priors are highly uncommon for objects such as t-shirts, desks, and many other observable items. Further, the colorization problem also inherits the typical challenges image enhancement, such as changes in illumination, variations in viewpoints, and occlusions.

In recent years, with the rapid development of deep learning techniques, a variety of image colorization models

have been introduced and state-of-the-art performance on current datasets has been reported. Diverse deep-learning models ranging from the early brute-force networks (*e.g.* [1]) to the recently carefully designed Generative Adversarial Networks (GAN) (*e.g.* [2]) have been successfully used to tackle the colorization problem. These colorization networks differ in many major aspects, including but not limited to network architecture, loss types, learning strategies, network depth, *etc.*

In this paper, we provide a comprehensive overview of single-image colorization and focus on the recent advances in deep neural networks for this task. To the best of our knowledge, no survey of either traditional or deep learning colorization has been presented in current literature. Our study concentrates on many important aspects, both in a systematic and comprehensive way, to benchmark the recent advances in deep-learning based image colorization.

**Contributions:** Our contributions are as follows

- 1) We provide a thorough review of image colorization techniques including problem settings, performance metrics and datasets.
- 2) We introduce a new benchmark dataset, named Natural-Color Dataset (NCD), collected specifically for the colorization task.
- 3) We provide a systematic evaluation of state-of-the-art models on our NCD.
- 4) We propose a new taxonomy of colorization networks based on the differences in domain type, network structure, auxiliary input, and final output.
- 5) We also summarize the vital components of networks, provide new insights, discuss the challenges, and possible future directions of image colorization.

**Related Surveys:** Image colorization has been the focus of significant research efforts over the last two decades while most early image colorization methods were primarily influenced by conventional machine learning approaches [3], [4], [5], [6], [7], [8] - the past few years have seen a huge shift

- *S. Anwar is a Research Scientist with Data61-CSIRO, Australia, and Lecturer at Australian National University, Australia. saeed.anwar@csiro.au*
- *M. Tahir is an Assistant Professor at College of Computing and Informatics, Saudi Electronic University. m.tahir@seu.edu.sa*
- *Chongyi Li is with the School of Computer Science and Engineering, Nanyang Technological University (NTU), Singapore. lichongyi25@gmail.com*
- *Ajmal Mian is a Professor of Computer Science with The University of Western Australia. ajmal.mian@uwa.edu.au*
- *Fahad S. Khan is a Lead Scientist at the Inception Institute of Artificial Intelligence (IIAI), Abu Dhabi, UAE and an Associate Professor at Computer Vision Laboratory, Linkoping University, Sweden. fahad.khan@liu.se*
- *Abdul W. Muzaffar is an Assistant Professor at College of Computing and Informatics, Saudi Electronic University. a.muzaffar@seu.edu.sa*
- *\* denotes equal contribution.*

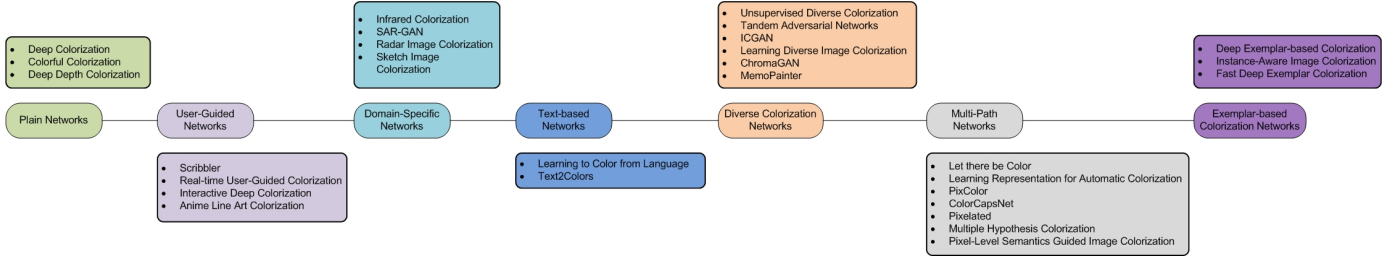


Fig. 1. **Taxonomy:** Classification of the colorization networks based on structure, input, domain, and type of network.

in focus to deep learning-based models due to their success in a number of different application domains [1], [9], [10], [11], [12].

Automatic image colorization systems built upon deep-learning methodologies have recently shown impressive performance. However, despite this success, no literature survey or review covering the latest developments in this field currently exists. Therefore, inspired by surveys in deep image super-resolution [13], VQA [14], *etc.* we aim to provide a survey for deep image colorization.

**Problem Formulation:** The aim of colorization is to convert a grayscale image to color image, typically captured in previous decades, when technological advancements were limited. Hence this process is more a form of image enhancement than image restoration. It is also possible that the color images such as RGB are converted to grayscale or Y-Channel of YUV color-space, possibly to save storage space or communication bandwidth. The grayscale images may also exist due to old technology or low-cost sensors. Therefore, in this case, a trivial formulation can be written as:

$$I_g = \Phi(I_{rgb}), \quad (1)$$

where  $\Phi(\cdot)$  is a function that converts the RGB image  $I_{rgb}$  to a grayscale image  $I_g$ , for example as follows:

$$I_g = 0.2989 * I_r + 0.5870 * I_g + 0.1140 * I_b. \quad (2)$$

Typically, colorization methods aim to restore the color in YUV space, where the model needs to predict only two channels, *i.e.* U and V - instead of the three channels in RGB.

## 2 SINGLE-IMAGE DEEP COLORIZATION

This section introduces the various deep learning techniques for image colorization. As shown in Figure 1, these colorization networks have been classified into various categories, in terms of different factors, such as structural differences, input type, user-assistance *etc.* Some networks may be eligible for multiple categories; however, we have simply placed these in the most appropriate category.

### 2.1 Plain Networks

Like in other CNN tasks, early colorization architectures were plain networks. We classify a network as plain if it possesses a simple, straightforward architecture with stacked convolutional layers, *i.e.*, no, or naive skip connections. Networks that fall into this category are shown in Figure 2 and are discussed below.

#### 2.1.1 Deep Colorization

Deep colorization<sup>1</sup> [1] can be regarded as the first work to have attempted to incorporate convolutional neural networks (CNNs) for the colorization of images. However, this method does not fully exploit the CNNs; instead, it also includes joint bilateral filtering [15] as a post-processing step to remove artifacts introduced by the CNN network.

In the training step, five fully connected linear layers are followed by non-linear activations (ReLU). The loss function utilized is the least-squares error. In the proposed model, the number of neurons in the first layer depends on the dimensions of the feature descriptor extracted from the grayscale patch, while the output layer has only two neurons, *i.e.*, the U and V channel corresponding color pixel value. In the testing step, features are extracted from the input grayscale image at three levels *i.e.* low-level, mid-level, and high-level. The features at low-level are the sequential gray values, at mid-level they are DAISY features [16], and at high-level semantic labeling is performed. The patch and DAISY features are concatenated and then passed through the network. As a final step for removing artifacts, joint bilateral filtering [15] is performed.

The network takes as input a  $256 \times 256$  grayscale image and is composed of five layers: one input layer, three hidden layers, and one output layer. The model is trained on 2688 images from the Sun dataset [19]. The images are segmented into 47 objects categories including cars, buildings, sea *etc.* for 47 high-level semantics. Furthermore, 32-dimensional mid-level DAISY features [16] and 49-dimensional low-level features are utilized for colorization.

#### 2.1.2 Colorful Colorization

Colorful image Colorization CNN<sup>2</sup> [18] was one of the first attempts to colorize grayscale images. The network takes as input a grayscale image and predict 313 “ab” pairs of the gamut showing the empirical probability distribution, which are then transformed to “a” and “b” channels of the “Lab” color space. The network stacks convolutional layers in a linear fashion, forming eight blocks. Each block is made up of either two or three convolutional layers followed by a ReLU layer and Batch Normalization (BatchNorm [20]) layer. Striding instead of pooling is used to decrease the size of the image. The input to the network is  $256 \times 256$ , while the output is  $224 \times 224$ ; however, it is resized later to the original image size.

1. Code available at <https://shorturl.at/cestD>

2. Code at <https://github.com/richzhang/colorization>

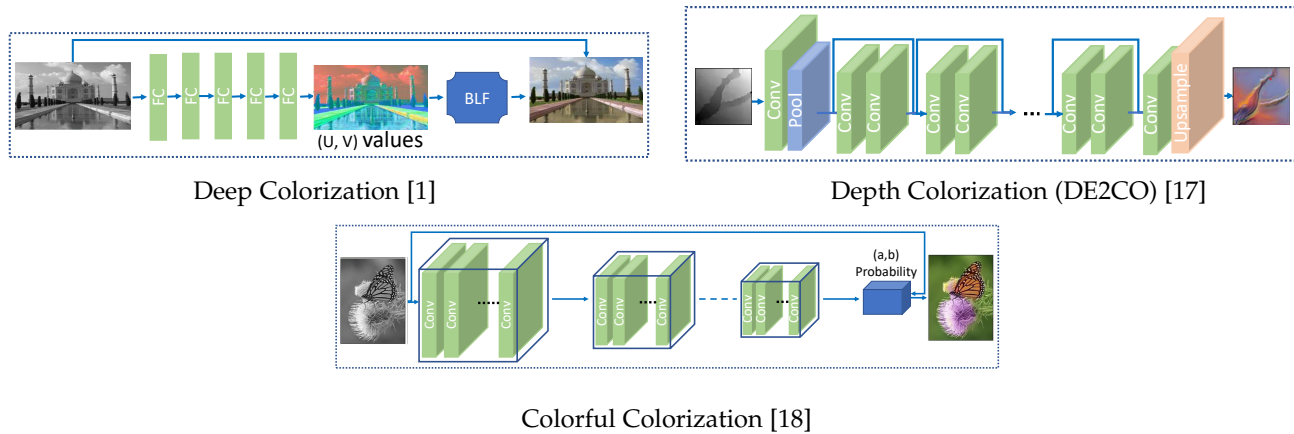


Fig. 2. **Plain networks** are the earlier models with convolutional layer stacking with no skip or naive skip connections.

The colorful image colorization network removes the influence (due to background, *e.g.* sky, clouds, walls *etc.*) of the low “ab” values by reweighting the loss based on the pixel rarity in training—the authors’ term this technique as class rebalancing.

The framework utilized to build the network is Caffe [21], and ADAM [22] is used as the solver. The network is trained for 450k iterations with a learning rate of  $3 \times 10^{-5}$ , which is reduced to  $10^{-5}$  at 200k and  $3 \times 10^{-6}$  at 375k iterations. The kernel size is  $3 \times 3$ , and the feature channels vary from 64 to 512.

### 2.1.3 Deep Depth Colorization

Deep depth colorization<sup>3</sup> (DE)<sup>2</sup>CO [17] employs a deep neural network architecture for colorizing depth images utilizing pre-trained ImageNet [23]. The system is primarily designed for object recognition by learning the mapping from the depths to RGB channels. The weights of the pre-trained network are kept frozen, and only the last fully connected layer of (DE)<sup>2</sup>CO is trained that classifies the objects with a softmax classifier. The pre-trained networks are merely used as feature extractors.

The input to the network is a  $228 \times 228$  depth map reduced via convolution followed by pooling to  $64 \times 57 \times 57$ . Subsequently, the features are passed through a series of residual blocks, composed of two convolutional layers, each followed by batch normalization [20] and a non-linear activation function *i.e.* leaky-ReLU [24]. After the last residual block, the output is passed through a final convolutional layer to produce three channels, *i.e.*, an RGB image as an output. To obtain the original resolution, the output is deconvolved as a final step. When an unseen dataset is encountered, only the last convolutional layer is retrained while keeping the weights across all other layers frozen. (DE)<sup>2</sup>CO outperforms CaffeNet (a variant of Alexnet [25]), VGG16 [26], GoogleNet [27], and ResNet50 [28] under the same settings on three benchmark datasets including Washington-RGBD [29], JHUIT50 [30], and BigBIRD [31].

## 2.2 User-guided networks

User-guided networks require input from the user either in the form of in points, strikes, or scribbles, as presented in Figure 3. The user input can be provided in real-time or offline. The following are examples of user-guided networks.

### 2.2.1 Scribbler

Sangkloy *et al.* [32] used an end-to-end feed-forward deep generative adversarial architecture<sup>4</sup> to colorize images. To guide structural information and color patterns, user input in the form of sketches and color strokes is employed. The adversarial loss function enables the network to colorize the images more realistically.

The generator part of the proposed network adopts an encoder-decoder structure with residual blocks. Following the architecture of Sketch Inversion [33], the augmented architecture consists of three downsampling layers, seven residual blocks preceded by three upsampling layers. The downsampling layers apply convolutions of stride two, whereas the upsampling layers utilize bilinear upsampling to substitute the deconvolutional layers contrary to Sketch Inversion. All layers are followed by batch normalization [20] and the ReLU activation function except the last layer, where the *TanH* function is used. The discriminator part of the proposed network is composed of a fully convolutional network with five convolutional layers and two residual blocks. Leaky-ReLU [24] is used after each convolutional layer except the last one, where Sigmoid is applied.

The proposed model’s performance is assessed qualitatively on datasets from three different domains, including faces, cars, and bedrooms.

### 2.2.2 Real-Time User-Guided Colorization

Zhang *et al.* [34] developed user interaction based on two variants, namely local hint and global hint networks, both of which utilize a common main branch for image colorization<sup>5</sup>. The local hint network is responsible for processing the user input and yielding color distribution, whereas the

3. Available at <https://github.com/engharat/SBADAGAN>

4. <https://github.com/Pingxia/ConvolutionalSketchInversion>

5. <https://github.com/junyanz/interactive-deep-colorization>

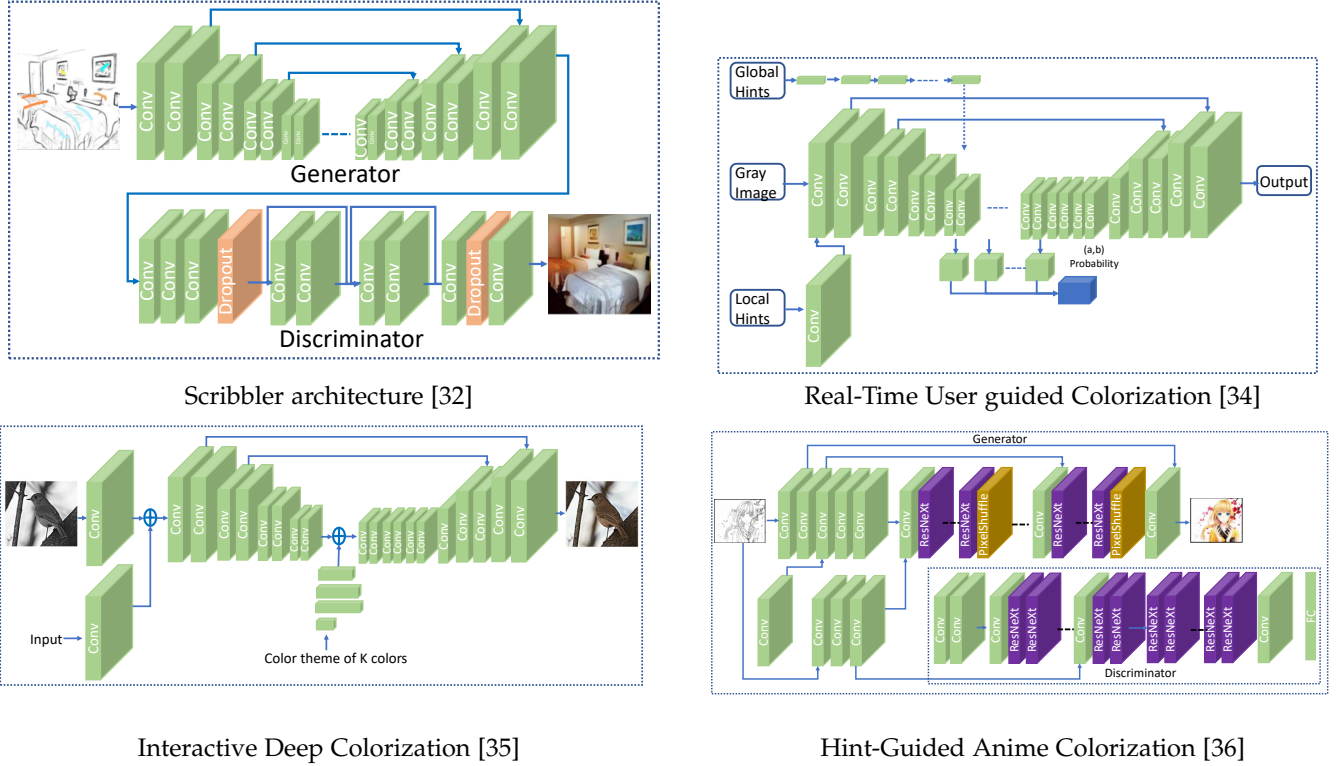


Fig. 3. **User-Guided networks** are the ones that require a user to input the color at some stage of the network during colorization.

global hint network accepts global statistics in the form of a global histogram and average saturation of the image. The loss functions include Huber and regression.

The main network is composed of ten blocks, made up of two or three convolutional layers followed by the ReLU. Similarly, each block is succeeded by batch normalization as well. In the first four blocks, feature tensors are continuously halved, while doubling the feature dimensions. The same process is performed in reverse order for the last four convolutional blocks. Moreover, a dilated convolution (with a factor of two) is applied for the fifth and sixth blocks. Symmetric shortcut connections are also established between different blocks for the recovery of spatial information. The kernel size for all convolutions is set to  $3 \times 3$ . However, a  $1 \times 1$  kernel is used at the last layer, mapping block ten and the final output.

### 2.2.3 Interactive Deep Colorization

To colorize grayscale images, Xiao *et al.* [35] developed an interactive colorization model based on the U-Net [37] architecture, which can simultaneously utilize global and local inputs. The network includes a feature extraction module, a dilated module, a global input module, and a reconstruction module.

The feature extraction module (layers 2 to 14) receives the inputs *i.e.* a grayscale image, local input, and gradient map that are merged via element-wise summation. The global input is processed by four convolution layers independently and then merged with the output of the feature extraction module using element-wise summation. The dilated module takes the input from the extraction module (corresponding to convolutional layers ranging from 15 to

20). The dilated module's output is further processed by a reconstruction module composed of many deconvolution and convolution layers. As a final step, the output of the network is combined with the input grayscale image to generate the colorized version. All the layers use ReLU except the final one, which employs a *TanH* activation.

The Huber loss is modified to meet the requirements of the proposed model. The testing set is composed of randomly chosen 1k images from ImageNet [23]. The proposed model is trained for 300k iterations utilizing the remaining images from ImageNet [23], combined with 150k images from Places dataset [38].

### 2.2.4 Anime Line Art Colorization

Ci *et al.* [36] proposed an end-to-end interactive deep conditional GAN (CGAN) [39] for the colorization of synthetic anime line arts. The system operates on the user hints and the grayscale line art.

The discriminator is conditioned on the local features computed from a pre-trained network called Illustration2Vec [40]. The generator adopts the architecture of U-Net [37] that has two convolution blocks and the local feature network at the start. Afterward, four sub-networks with similar structures are employed, each of which is composed of convolutional layers at the front followed by ResNeXt blocks [41] with dilation and sub-pixel convolutional (PixelShuffle) layers. Each convolutional layer utilizes LeakyReLU as activation function, except the final one where *TanH* activation is employed. The discriminator, on the other hand, is inspired by the architecture of SRGAN [42]; however, the basic blocks are replaced from

the earlier mentioned generator to remove dilation and an increased number of layers is used.

The generator employs the perceptual and adversarial losses, and the discriminator combines Wasserstein critic and penalty losses. The ADAM [22] optimizer is employed with  $\beta_1 = 0.5$ ,  $\beta_2 = 0.9$  and a batch size of four.

## 2.3 Domain-Specific Colorization

The aim of these networks is to colorize images from different modalities such as infrared, or different domains such as radar. We provide the details of such networks in the following sub-sections and are shown in Figure 4.

### 2.3.1 Infrared Colorization

An automatic Near Infrared (NIR)<sup>6</sup> image colorization technique [43] was developed using a multi-branch deep CNN. NIR [43] is capable of learning luminance and chrominance channels. Initially, the input image is preprocessed and is converted into a pyramid. Where each pyramid-level is normalized *i.e.* has zero mean and unit variance. Next, each structurally similar branch of NIR [43] is trained using a single input pyramid-level without sharing weights between layers. All the branches are merged into a fully connected layer to produce the final output. Additionally, the mean input image is also fed directly to the fully connected layer.

The fundamental structure of NIR is inspired by [18]. Each branch is composed of stacked convolutional layers with pooling layers placed in the middle after regular intervals. The activation function after each convolutional layer is ReLU. In order to produce the colorized image, the raw output of the network is joint-bilaterally filtered, and the output is then further enhanced by incorporating high-frequency information directly from the original input image.

Each block has the same number of convolutional layers. The kernel size is  $3 \times 3$ , while a downsampling of  $2 \times 2$  is utilized in the pooling layers. Similarly, the same number of feature maps, *i.e.* 16, are employed in the first block, but after each pooling layer, the number is increased by 2. Moreover, The authors developed a real-world dataset by capturing road scenes in summer with a multi-CCD NIR/RGB camera. The proposed model is trained on about 32 image pairs and tested on 800 images from the mentioned dataset.

### 2.3.2 SAR-GAN

To colorize Synthetic Aperture Radar (SAR) images, Wang *et al.* [46] proposed SAR-GAN. The network uses a cascaded generative adversarial network as its underlying architecture. The input SAR images are first denoised from speckles and then colorized to produce high-quality visible images. The generator of SAR-GAN [46] consists of a despeckling subnet and colorization subnet. The output of the despeckling subnet is a noise-free SAR image that is further processed by the colorization subnet to produce a colorized image.

The despeckling sub-network consists of eight convolutional layers with batch normalization [20], an activation function, and an element-wise division residual layer. First,

the speckle component in the SAR image is estimated and forwarded to the residual layer. To generate a noise-free image, a residual layer equipped with skip connections performs component-wise division of the input SAR image by the estimated speckle. The colorization sub-network utilizes a symmetric encoder-decoder architecture with eight convolutional layers and three skip connections that enable the network's input and output to share low-level characteristics.

The ADAM [22] optimization technique is adopted for training the entire network. The discriminator component of SAR-GAN [46] utilizes a hybrid loss function, developed by combining the pixel-level  $\ell_1$  loss with the adversarial loss. SAR-GAN [46] is tested on 85 out of 3292 synthetic images as well as real SAR images. .

### 2.3.3 Radar Image Colorization

Song *et al.* [45] developed a feature-extractor network and a feature-translator network for the colorization of single-polarization radar grayscale images<sup>7</sup>. To construct the feature-extractor network, the first seven layers of the VGG16 [26] pre-trained on ImageNet [23], are used. The output of the feature extractor network is in the form of a hyper-column descriptor that is obtained by concatenating the corresponding pixels from all layers along with the input image.

The final hyper-column descriptor, thus obtained, is fed into the feature-translator network that is composed of five fully connected layers. As a final step, the feature-translator network uses softmax function to obtain the output similar to classification, which is achieved by constructing nine groups of neurons representing nine polarimetric. The ReLU activation function follows each convolutional layer in both networks. Furthermore, to train both the feature-extractor and feature-translator, full polarimetric radar image patches are employed.

### 2.3.4 Sketch Image Colorization

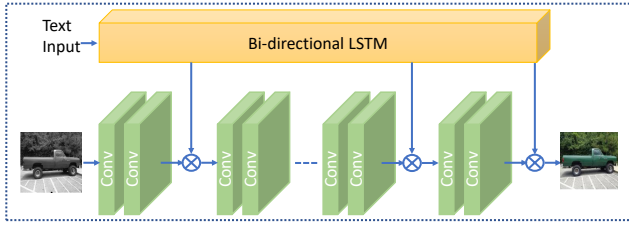
Lee *et al.* [44] proposed a reference-based sketch image colorization, where a sketch image is colorized according to an already-colored reference image. In contrast to grayscale images, which contain the pixel intensity, sketch images are more information-scarce, which makes sketch image colorization more challenging.

In the training phase, the authors proposed an augmented self-reference generation method, generated from the original image by both color perturbation and geometric distortion. Specifically, a color image is first converted into its sketch image using an outline extractor. Then, the augmented self-reference image is generated by applying the thin plate splines transformation to the reference image. The generated reference image as the ground truth contains most of the content from the original image, thus, providing a full information of correspondence for the sketch. Taking the sketch image and reference image as inputs, the network first encodes these two inputs by two independent encoders. Furthermore, the authors proposed a spatially corresponding feature transfer module to transfer the contextual representations obtained from the reference into the spatially

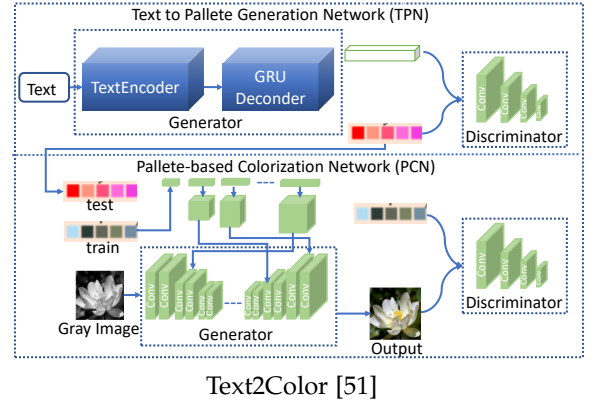
6. Code is available at <https://bit.ly/2YZQhQ4>

7. Code at <https://github.com/fudanxu/SAR-Colorization>





LCL-Net architecture [47]



Text2Color [51]

Fig. 5. **Text-based colorization networks** are based on the text input with the grayscale image.

The TPN generator learns the pairing between text and color palette, while its discriminator, simultaneously learns the characteristics of the color palette and text, to identify the real palettes from the fake ones. The loss function in the TPN network is the Huber loss.

On the other hand, the generator of the PCN network has two subnetworks: the colorization network based on U-Net [37] to colorize the images and the conditioning network to apply the palette colors to the generated image. The PCN discriminator is based on the DCGAN architecture [52]. In the PCN’s discriminator, first, the features from the input image and generated palette (by the TPN network) are jointly learned by a series of Conv-LeakyReLU layers. Then, a fully connected layer classifies the image as either real or fake.

The discriminator and generator of TPN are first trained on the PAT dataset for 500 epochs, and then trained on the ground-truth image for 100 epochs. The trained generators of TPN and PCN are then used to colorize the input grayscale image at the testing stage using the input text’s color palette. Adam optimizer is used with a learning rate of 0.0002 for all the networks. Input text’s color palette. Adam optimizer with a learning rate of 0.0002 for all the networks.

## 2.5 Diverse Colorization

The aim of diverse colorization is to generate different colorized images, rather than restore the original color shown in Figure 6. Diverse colorization is usually achieved via GANs or variational autoencoders. GANs attempt to generate the colors in a competitive manner where the Generator tries to fool the Discriminator while the Discriminator tries to differentiate between the ground-truth and the generated colors. We present the vanilla GANs employed for colorization.

### 2.5.1 Unsupervised Diverse Colorization

Cao *et al.* [53] proposed the utilization of conditional GANs for the diverse colorization of real-world objects<sup>10</sup>. In the generator of the proposed GAN network, the authors employed five fully convolutional layers with batch normalization and ReLU. To provide continuous conditional supervision for realistic results, the grayscale image is concatenated

with every layer of the generator. Furthermore, to diversify the colorization outputs, noise channels are added to the first three convolutional layers of the generator network. The discriminator is composed of four convolutional layers and a fully-connected layer to differentiate between the fake and the real values of the image.

During the convolution operations, the stride is set to 1 to keep the spatial information the same across all layers. The performance of the proposed method was assessed using the Turing test methodology. The authors provided questionnaire surveys to 80 subjects asking them 20 different questions regarding the produced results for the publicly available LSUN bedroom dataset [54]. The proposed model obtained a convincing rate of 62.6% compared to 70% for ground-truth images. Additionally, a significance t-test generated a p-value of 0.1359, indicating that the generated colorized images are not significantly different from the real images.

For implementation, the authors opted for the TensorFlow framework. The batch size was selected as 64 with a learning rate of 0.0002 and 0.0001 for the discriminator and generator, respectively. The model was trained for 100 epochs using RMSProp as an optimizer. The output of the network is  $64 \times 64$  in size.

### 2.5.2 Tandem Adversarial Networks

For the colorization of raw line-art, Frans [55] proposed two adversarial networks in tandem. The first network, namely the color-prediction network, predicts the color scheme from the outline, while the second network, called the shading network, produces the final image from the color scheme generated by the color-prediction network in conjunction with the outline. Both the color-prediction and shading networks have same structure as U-Net [37] while the discriminator has the same structure as [53]. The adversarial training is performed using the discriminator formed by stacking the four convolutional layers and a fully connected layer at the end.

The convolutional layers are transposed once the density of the feature matrix reaches a certain level. The author also added skip connections between the corresponding layers to directly allow the gradient to flow through the network. Further,  $\ell_2$  and adversarial losses are incorporated in the color-prediction and shading-networks, respectively.

10. Code is available at <https://github.com/ccyyatnet/COLORGAN>

The convolutional filter size is set to  $5 \times 5$  with a stride of two for every convolutional layer in the network. The number of feature maps is increased by two times after every layer, where the initial number of feature maps is 64.

### 2.5.3 ICGAN

Image Colorization Using Generative Adversarial Networks, abbreviated as ICGAN [56] proposed by Nazeri *et al.*, has demonstrated better performance in image colorization tasks than traditional convolutional neural networks. Fully convolutional networks for semantic segmentation [59] inspire the baseline model and is constructed by replacing the fully connected layers of the network by fully convolutional layers. The basic idea is to downsample the input image gradually via multiple contractive encoding layers and then apply a reverse operation to reconstruct the output with many expansive decoding layers, similar to U-Net [37].

The ICGAN [56] generator takes grayscale input image as opposed to random noise, like traditional GANs. The authors also proposed the generator’s modified cost function to maximize the discriminator’s probability of being incorrect instead of minimizing the likelihood of being correct. Moreover, the baseline model’s generator is used without any modifications, while the discriminator is composed of a series of convolutional layers with batch normalization [20].

The filter size in each convolutional layer is  $4 \times 4$  as opposed to the traditional  $3 \times 3$ , and the activation function is Leaky-ReLU [24] with a slope value of 0.2. The final one-dimensional output is obtained by applying a convolution operation after the last layer, predicting the input’s nature with a certain probability.

To train the network, the authors employed ADAM optimization [22] with weight initialization using the guidelines from [60]. The performance of the system is assessed using CIFAR10 [61] and Places356 datasets [62]. Overall, the visual performance of the ICGAN [56] is favorable compared to that of traditional CNN.

### 2.5.4 Learning Diverse Image Colorization

Deshpande *et al.* [57] employed Variational Auto-Encoder (VAE) and Mixture Density Network (MDN) to yield multiple diverse yet realistic colorizations for a single grayscale image<sup>11</sup>. The authors first utilized VAE to learn a low-dimensional embedding for a color field of size  $64 \times 64 \times 2$ , and then the MDN was employed to generate multiple colorizations.

The VAE architecture encoder consists of four convolutional layers with a kernel size of  $5 \times 5$  and stride of two. The feature channels start at 128 and double in the successive encoder layer. Each convolutional layer is followed by batch normalization, and ReLU is used as an activation function. The last layer of the encoder is fully connected. On the other hand, the decoder of the VAE architecture has five convolutional layers, each one preceded by linear upsampling and followed by batch normalization, and ReLU. The input to the decoder is a  $d$ -dimensional embedding, and the output is a  $64 \times 64 \times 2$  color field. The convolutional kernel size is  $4 \times 4$  in the first layer, and in the remaining, it is of size  $5 \times 5$ . As mentioned earlier, activation function in all layers is

ReLU, except in the last layer, where the activation function is *TanH*. The output channels at each layer are halved in the decoder.

MDN consists of twelve convolutional layers and two fully connected layers and is activated by the ReLU function, which is followed by batch normalization. During the testing embeddings sampled from the MDN output can be used by the Decoder of the VAE to produce multiple colorizations. To enhance the overall performance of the proposed architecture, the authors designed three loss functions: specificity, colorfulness, and gradient.

### 2.5.5 ChromaGAN

ChromaGAN<sup>12</sup> [58] exploits geometric, perceptual, and semantic features via an end-to-end self-supervised generative adversarial network. By utilizing the semantic understanding of the real scenes, the proposed model can colorize the image realistically (actual colors) rather than merely pleasing the human eyes.

The Generator of ChromaGAN [58] is composed of two branches, which receive a grayscale image of size  $224 \times 224$  as input. One of the branches yields chrominance information, whereas the other generates a class distribution vector. The network composition is as follows: the first stage is shared between both the branches that implements VGG16 [26] while removing the last three fully connected layers. The pre-trained VGG16 [26] weights are used to train this stage without freezing them. In the second stage, each branch follows its dedicated path. The first branch has two modules, each one designed by combining a convolutional layer followed by Batch normalization [20] and ReLU. The second path has four modules with the same composite structure (Conv-BN-ReLU) as of the first branch but is further followed by three fully connected layers and provides the class distribution. In the third stage, the outputs of these two distinct paths fused. The features then pass through six modules. Each module has a convolutional layer and ReLU with two upsampling layers within.

The discriminator is based on PatchGAN [63] architecture that holds high-frequency structural information of the generator’s output by focusing on the local patches rather than the entire image. ChromaGAN [58] is trained on 1.3M images of ImageNet [23] for a total of five epochs. The optimizer used is ADAM with an initial learning rate of  $2e^{-5}$ .

### 2.5.6 MemoPainter: Coloring with Limited Data

MemoPainter<sup>13</sup> [2] is capable of learning from limited data, which is made possible by the integration of external memory networks [64] with the colorization networks. This technique effectively avoids the dominant color effect and preserves the color identity of different objects.

Memory networks keep the history of rare examples, enabling them perform well even with insufficient data. To train memory networks in an unsupervised manner, a novel threshold triplet loss was introduced by the authors [2]. In memory networks, the “key-memory” holds spatial information and computes cosine similarity against

11. Code is available at <https://github.com/aditya12agd5/divcolor>

12. Code available at <https://github.com/pvitoria/ChromaGAN>

13. <https://github.com/dongheehand/MemoPainter-PyTorch>

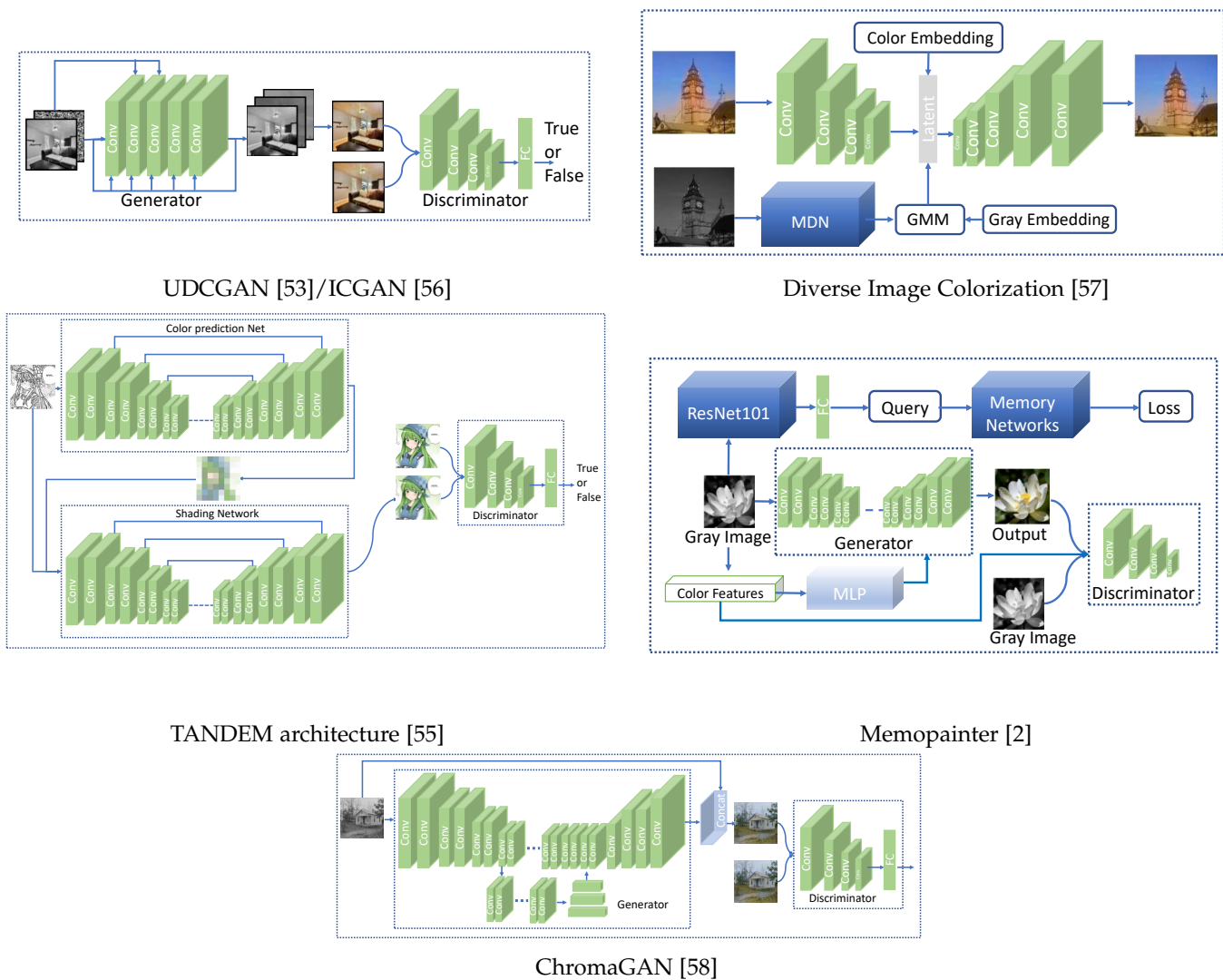


Fig. 6. **Diverse colorization networks** generate different colored images instead of aiming to restore the original color only.

the input. Likewise, “value-memory” keep records about color information utilized by the colorization networks as a condition. Similarly, “age” keeps the time-stamp for each entry in the memory. The “key” and “value” memories are generated from the training data. The memory is updated by averaging the “key-memory” and a new query image owing to the distance between the color information of the new query image and the available top-1 “value-memory” element lies below the threshold. Otherwise, a new record is stored for the input image color information.

The colorization networks are constructed using conditional GANs [39] consisting of a generator and discriminator, and color information is learned from RGB images during training. The generator inspired by U-Net [37], is composed of ten convolutional layers, while the discriminator is fully convolutional, consisting of four layers. The color feature is extracted and provided to the generator after being passed forward from the MLP.

During testing, the color information is retrieved from the memory networks and fed to the generator as a condition. The colorization networks employ adaptive instance

normalization for enhanced colorization as it is considered as a style transfer. The performance of MemoPainter [2] is evaluated on different datasets, including Oxford102 Flower [65], Monster [66], Yumi<sup>14</sup>, Superheroes [2], and Pokemon<sup>15</sup>.

## 2.6 Multi-path networks

The multi-path networks follow different parts to learn features at different levels or different paths. The following are examples of multi-path networks, and Figure 7 provides their architectures.

### 2.6.1 Let there be Color

Iizuka *et al.* [67] designed a neural network<sup>16</sup> to primarily colorize the grayscale images and provide scene classification as a secondary task. The proposed system has two branches to learn features at multiple scales. Both branches

14. <https://comic.naver.com/webtoon/list.nhn?titleId=651673>

15. <https://www.kaggle.com/kvpratama/pokemon-images-dataset>

16. [https://github.com/satoshiizuka/siggraph2016\\_colorization](https://github.com/satoshiizuka/siggraph2016_colorization)

are further divided into four subnets, *i.e.* the low-level features subnet, mid-level features subnet, global features subnet, and colorization network. The low-level subnet decreases the resolution and extract edges and corners. To learn the textures, mid-level features come in handy.

Similarly, a 256D vector is computed by the global subnet to represent the image. The mid-level and global features are combined and fed into the colorization network to predict the chrominance channel. The final output is restored to the original input resolution. The global features help the classification network to classify the scene in the image. Both the colorization network and scene classification network are jointly trained.

The low-level features subnet is composed of six convolution layers, the mid-level features subnet has two convolutional layers, and the global features network is comprised of four convolutional layers as well as three fully-connected layers. The colorization network is made up of a fusion layer, four convolutional, and two upsampling layers. To feed input to the network, the image is resized to  $256 \times 256$ , and then output is upsampled to its original resolution. The kernel is of size  $3 \times 3$ ; feature channels vary between 64 to 512, and striding is used to reduce the feature map size. Moreover, the learning rate is determined automatically using ADADELTA [68], the network is optimized using Stochastic Gradient Descent (SGD) [69], and the system is designed using Torch [70].

### 2.6.2 Learning Representations for Automatic Colorization

Learning Representations for Automatic Colorization<sup>17</sup> [71] aims to learn a mapping function taking per-pixel features as hypercolumns of localized slices from existing CNN networks to predict hue and chroma distributions for each pixel. The authors use VGG16 [26] as a feature extractor while discarding the classification layer and using a grayscale image as input rather than RGB. For each pixel, a hypercolumn is extracted from all the VGG16 layers except the last classification layer resulting in a 12k channel feature descriptor that is fed into a fully connected layer of 1k channels, which predicts the final hue and chroma outputs.

The KL divergence is employed as a loss to predict distributions over a set of color bins. The input size is  $256 \times 256$ , and the framework used is Caffe [21], where the network is fine-tuned for ten epochs, each of which takes about 17 hours. Other parameters and optimizations are similar to VGG16 [26].

### 2.6.3 PixColor

PixColor, proposed by [72], employs a conditional PixelCNN to produce a low-resolution color image from a given grayscale image. Then, a refinement CNN is then trained to process the original grayscale and the low-resolution color image to produce a high-resolution colorized image. The colorization of an individual pixel is determined by the color of the previous pixels.

PixelCNN is composed of two convolutional layers and three ResNet blocks [28]. The first convolutional layer uses kernels of size  $7 \times 7$  while the last one employs  $3 \times 3$ . Similarly, ResNet blocks contain 3, 4, and 23 convolutional

layers, respectively. The PixelCNN colorization network is composed of three masked convolutional layers: one in the beginning and second at the end of the network, whereas a Gated convolutional Block with ten layers is surrounded by the Gated convolutional layers.

The PixelCNN model is trained by applying a maximum likelihood function with cross-entropy loss. Then, the refinement network - composed of 16 convolutional layers followed by two bilinear upsampling layers, each with two internal convolutional layers - is trained on the ground-truth chroma images downsampled to  $28 \times 28$ . The network ends with three convolutional layers, where the final layer outputs the colorized image.

### 2.6.4 ColorCapsNet

Colorize Capsule Network (ColorCapsNet) [76] is built upon CapsNet [77] with three modifications. Firstly, the single convolutional layer is replaced by the first two convolutional layers of VGG19 [26] and initialized via its weights. Secondly, Batch normalization [20] is inserted in between the first two convolutional layers. Thirdly, the number of capsules is reduced from ten to six in the capsule layer. The architecture of ColorCapsNet is similar to an autoencoder. The colorization specific hidden variables are in between the encoder and decoder, are processed in the latent space.

To train the model, the input RGB image is first converted into the CIE Lab colorspace, and extracted patches are fed to the network in order to learn the color distribution. The output is in the form of colorized patches which are combined to obtain the complete image in Lab colorspace and later converted to RGB colorspace.

The difference between real and generated images is minimized using the Mean Squared Error loss. ColorCapsNet is trained on ILSVRC 2012 to learn the general color distribution of objects and then be finetuned using the DIV2K dataset [78]. ColorCapsNet shows comparable performance to other models, despite its shallow architecture. Adam is used as the optimizer with a learning rate of 0.001 with different kernel sizes.

### 2.6.5 Pixelated

Pixelated, introduced by Zhao *et al.* [74] is an image colorization model guided by pixelated semantics to keep the colorization consistent across multiple object categories. The network architecture is composed of a color embedding branch and a semantic segmentation branch. The network is built from gated residual blocks, each of which contains two convolutional layers, a skip connection, and a gating mechanism.

The learning mechanism is composed of three components. *Firstly*, an autoregressive model, is adopted to utilize pixelated semantics for image colorization. A shared CNN is used for modeling to achieve colorization diversity by generating per-pixel distributions using a conditional PixelCNN. *Secondly*, semantic segmentation is incorporated into color embedding by introducing atrous spatial pyramid pooling at the top layer capable of extracting multi-scale features using several parallel filters. The output is obtained by fusing multi-scale features. The loss function for semantic

17. Code is available at <https://github.com/gustavla/autocolorize>

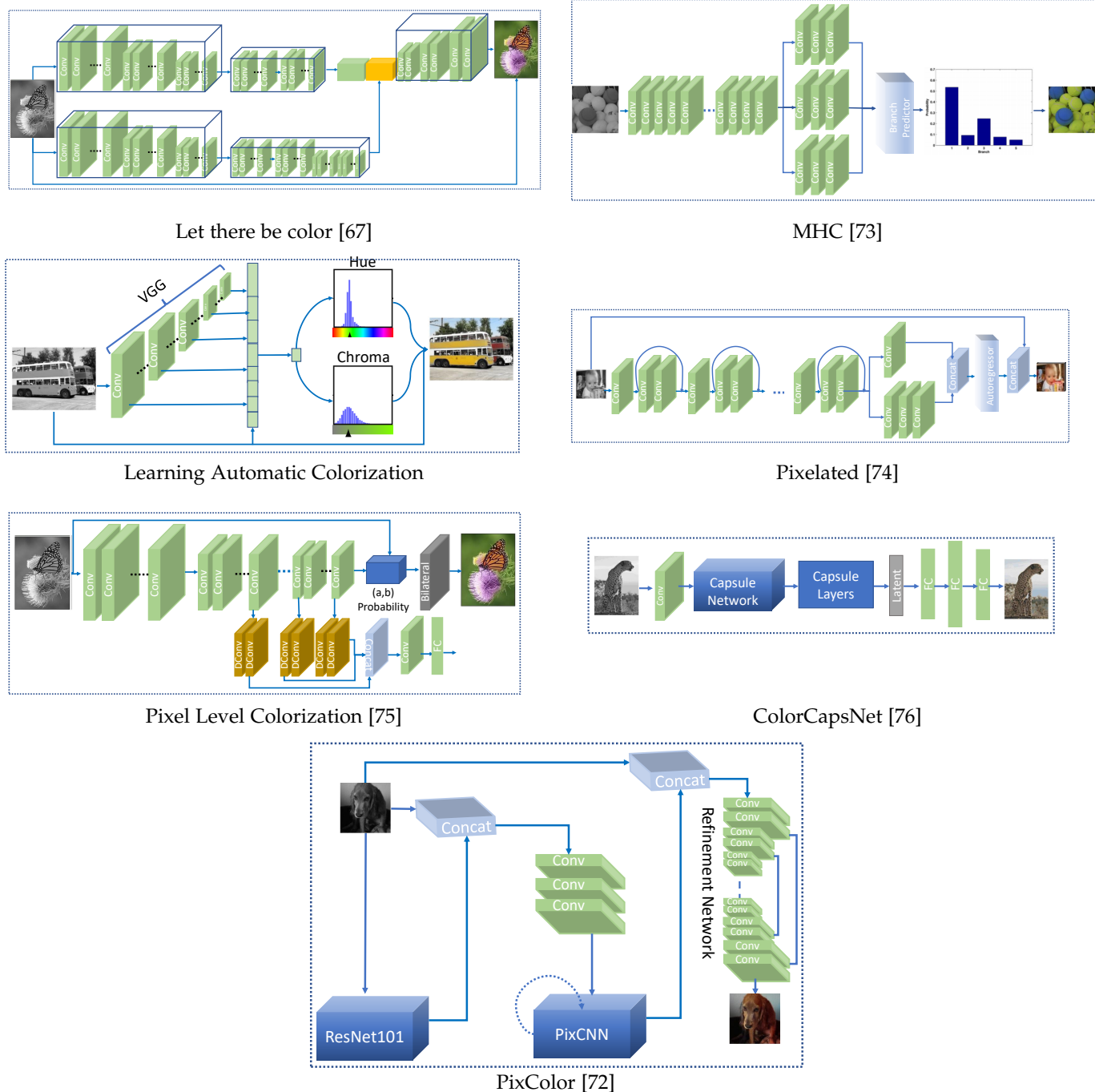


Fig. 7. **Examples of multi-path networks.** These colorization networks learn different features via several network paths.

segmentation is the cross-entropy loss with softmax function. *Thirdly*, to produce better and more accurate color distributions, pixelated color embedding is concatenated with semantic segmentation to create the semantic generator.

During training, color embedding loss, semantic loss, and color generation loss are combined. The performance of the network is evaluated on the Pascal VOC2012 [79] and COCO-stuff [50] datasets. The images are rescaled to  $128 \times 128$  for use in the network.

### 2.6.6 Multiple Hypothesis Colorization

Mohammad & Lorenzo [73] developed a multiple hypothesis colorization architecture, producing multiple color values for each pixel of the grayscale image. The low-cost colorization is achieved by storing the best pixel-level hypothesis. The shared features are computed by a common trunk consisting of convolutional layers. The trunk is then split into multiple branches where each branch predicts color for each pixel. The layers in the main trunk and its subsequent branches are all fully convolutional.

The authors developed two architectures, one for CIFAR100 and the other for ImageNet [23]. The architecture for

the CIFAR100 dataset is composed of 31 blocks preceded by a stand-alone convolutional layer. The number of channels in different layers across multiple blocks varies from 64 to 256. In contrast, the architecture for the ImageNet [23] is composed of 21 blocks in total. The number of channels across different layers inside blocks varies from 32 to 1024. Although the two models have a different number of blocks, the block structure is the same. Residual connections are also used in both networks. Moreover, batch normalization is performed in all blocks, and ReLU is applied to all layers, except the last of each block.

Softmax is employed as a loss function. The CIFAR100 model is trained for 40k iterations with a learning rate of 0.001, which is dropped after 10k and 20k iterations by a factor of 10. Similarly, the ImageNet [23] model is trained for 120k iterations with an initial learning rate of 0.0005 that is dropped after 40k and 80k iterations by a factor of 5.

### 2.6.7 Pixel-Level Semantics Guided Image Colorization

A hierarchical network comprised of a semantic segmentation branch and a colorization branch was developed by Zhao *et al.* [75]. The first four convolution layers are shared between the two branches to learn low-level features. Four more convolutional layers further extend the colorization branch, while three deconvolution layers from the segmentation branch. The output of the deconvolutional layers is concatenated and passed through the final convolutional layer to produce class probabilities.

Semantic segmentation is achieved through weighted cross-entropy loss and softmax function, whereas colorization is performed via multinomial cross-entropy loss with class rebalance. During the training, the network jointly optimizes the two tasks. During the testing, a joint bilateral upsampling layer is introduced to generate the final output.

For semantic segmentation, the model is trained on 10,582 and tested on 1449 images from the PASCAL VOC2012 dataset for 40 epochs. Similarly, 9k images are used for training and 1k images for testing on the COCO-stuff dataset [50] for 20 epochs.

## 2.7 Exemplar-based Colorization

Exemplar-based colorization utilizes the colors of example images provided along with input grayscale images. Figure 8 presents the example networks for exemplar-based colorization. We provide more details about the networks in the subsequent sub-sections.

### 2.7.1 Deep Exemplar-based Colorization

Deep exemplar-based colorization<sup>18</sup> [80] transfers the colors from a reference image to the grayscale one. The aim here is not to colorize images naturally but to provide diverse colors to the same image. The system is composed of two subnetworks: Similarity subnetwork and Colorization sub-network.

The similarity subnet takes the target and reference luminance channels aligned before via Deep Image Analogy [81]. The authors use the standard features of VGG19 [26] after each of its blocks resulting in coarse to fine, five levels

of feature maps. The features are upsampled to the same size. The similarity subnet computes a bidirectional similarity map using discrete cosine distance. Furthermore, the colorization subnet concatenates the grayscale image, chrominance channels, and the calculated similarity maps. U-Net [37] inspires the structure of the colorization subnet.

The loss function is  $\ell_2$ , which is a combination of chrominance channels and perceptual loss. The network is trained by employing ADAM optimizer [22] in the Caffe framework [21] with a learning rate of  $10^{-3}$  for ten epochs, reduced by 0.1 after 33% of training.

### 2.7.2 Fast Deep Exemplar Colorization

Current exemplar-based colorization methods suffer from two challenges: 1) they are sensitive to the selection of reference images, and 2) they have high time and resource consumption. Inspired by stylization characteristics in feature extracting and blending, Xu *et al.* [82] proposed a stylization-based architecture for fast deep exemplar colorization. The proposed architecture consists of two parts: a transfer subnet that learns a coarse chrominance map (ab map in CIE Lab color space) and a colorization sub-net that refines the map to generate the final colored result. The proposed method aims to generate plausible colorization results in real-time, whether the input and exemplar image are semantically related or not. More specifically, an encoder-decoder structure is used for the transfer sub-net, which takes the target-reference image pairs as the input and output initial ab map. The pre-trained VGG19 module (from *conv1*<sub>1</sub> layer to *conv4*<sub>1</sub> layer) is treated as the encoder and a symmetrical decoder for image reconstruction. In addition, the fast Adaptive Instance Normalization (AdaIN) [84] is utilized after convolutional layers to accelerate feature matching and blending. The ab map generated by the transfer sub-net is inaccurate and has some artifacts. To refine it, a colorization sub-net that adopts an analogous U-Net structure is designed, which takes a known luminance map along with initial chrominance ab map as input.

In the original implementations, the transfer sub-net is trained on the Microsoft COCO dataset [50] by minimizing the sum of the  $L_2$  loss while the colorization sub-net is trained on the ImageNet dataset [23] by minimizing the Huber loss [85].

### 2.7.3 Instance-Aware Image Colorization

The Existing colorization models usually fail to colorize the images with multiple objects. To solve this issue, Su *et al.* [83] proposed an instance-aware image colorization method<sup>19</sup>. The network includes three parts: 1) an off-the-shelf pre-trained model to detect object instances and produce cropped object images, 2) two backbone networks trained end-to-end for instance, and full-image colorization and 3) a fusion module to selectively blend features extracted from different layers of the two colorization networks. Specifically, a grayscale image as input is fed to the network. The network first detects the object bounding boxes using an off-the-shelf object detector. Then, each detected instance is

18. <https://github.com/msracver/Deep-Exemplar-based-Colorization>

19. Code is available at <https://cgv.cs.nthu.edu.tw/projects/instaColorization>

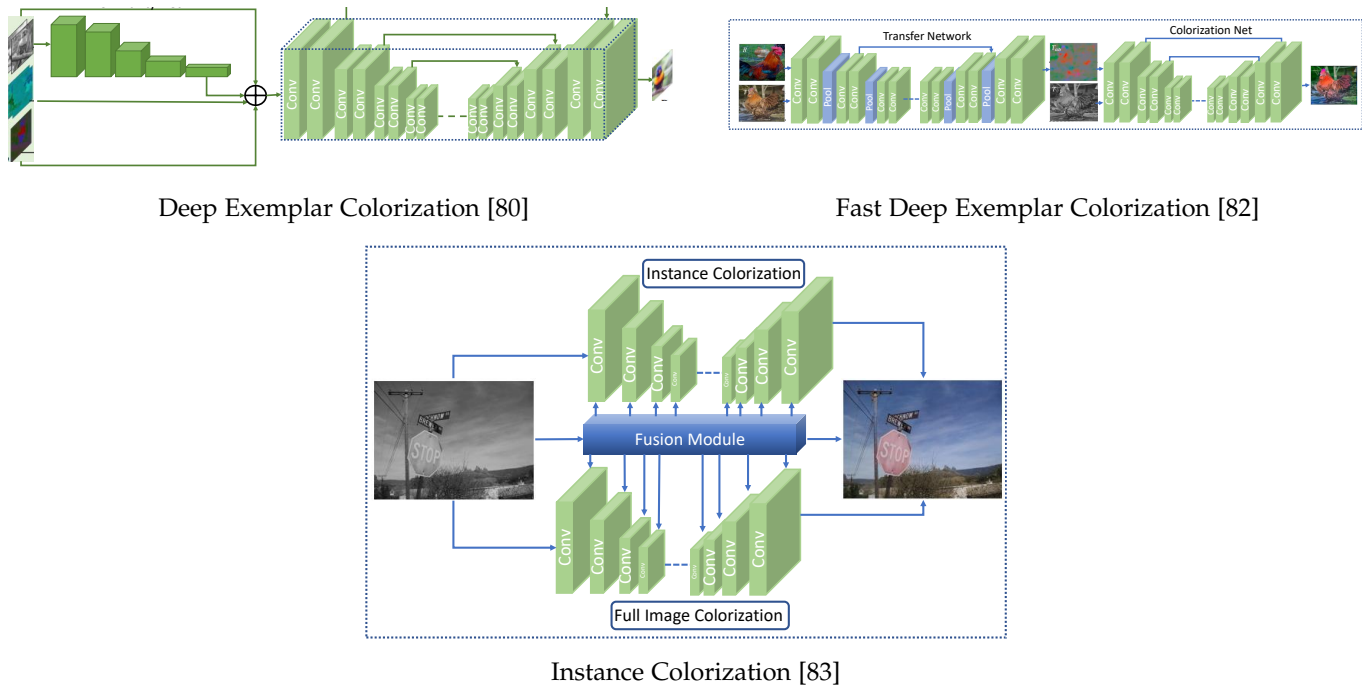


Fig. 8. **Exemplar-based Colorization networks.** These networks imitate the colors of the input example image provided along with the grayscale image.

cropped out and forwarded to the instance colorization network, for instance, colorization. At the same time, the input grayscale image is also sent to another instance colorization network (with same structure, but different weights) for full-image colorization. Finally, a fusion module is used to fuse all the instance features with the full-image feature at each layer until obtaining the output colored image. In the training phase, a sequential approach strategy that trains the full-image network followed by the instance network, and finally trains the feature fusion module by freezing the above two networks is adopted. The smooth- $L_1$  loss is used to train the network.

In the original implementation, the channel numbers of the full-image feature, instance feature, and fused feature in each of the 13 layers are 64, 128, 256, 512, 512, 512, 256, 256, 128, 128, 128, and 128. The authors use three datasets for training and evaluation, including ImageNet [23], COCO-Stuff [86], and Places205 [87]. Moreover, the images are resized to a size of  $256 \times 256$ .

### 3 EXPERIMENTS

#### 3.1 Datasets

The datasets available for evaluation are the most commonly used ones in the literature for other tasks such as detection, classification, segmentation *etc.* Where the images are first converted to grayscale, and then apply colorization models to analyze its performance. Hence, we provide a new dataset, explicitly designed for the colorization task in the next section, while We list the currently used datasets below.

- **COCO-stuff dataset [86]:** The Common Objects in Context-stuff (COCO-stuff) is constructed by annotating the original COCO dataset [50], which origi-

nally annotated things while neglecting stuff annotations. There are 164k images in COCO-stuff dataset that span over 172 categories including 80 things, 91 stuff, and 1 unlabeled class.

- **PASCAL VOC dataset [88]:** PASCAL Visual Object Classes (PASCAL VOC) dataset has more than 11000 images that are divided into 20 object categories.
- **CIFAR datasets [61]:** CIFAR-10 and CIFAR-100 are two subsets created and reliably labelled from 80 million tiny image dataset [89]. CIFAR-10 is comprised of 60k images equally distributed over mutually exclusive 10 categories with 6k images in each category. On the other hand, CIFAR-100 has the same images distributed over 100 categories with 600 images assigned to each category. Each image in both the subsets is of size  $32 \times 32$  pixels. In CIFAR-100, two level labelling is used. At the higher level there are 20 superclasses each of which is further divided into five subclasses. Overall, 50k and 1k images comprise training and testing sets, respectively.
- **ImageNet ILSVRC2012 [23]:** This dataset contains 1.2 million high resolution training images spanning over 1k categories where 50k images comprise the hold-out validation set. Images are rescaled to  $128 \times 128$  pixels.
- **Palette-and-Text dataset [51]:** is constructed by making modifications to the data collected from color-hex.com where users upload user-defined color palettes with label names of their choice. The authors first collected 47,665 palette-text pairs and removed non-alphanumeric and non-English words from the

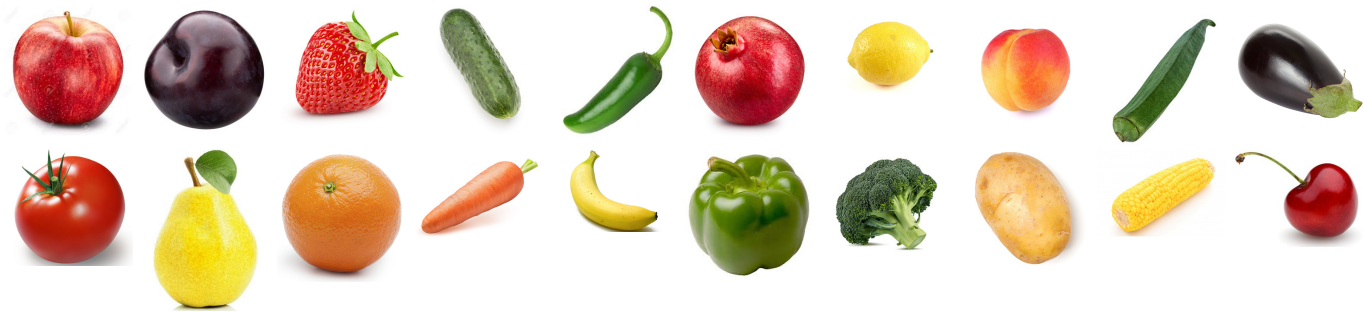


Fig. 9. Sample images for each category from our proposed Natural-Color dataset (NCD).

collection. After removing text-palette pairs that lack semantic relationships, the final curated dataset contains 10,183 textual phrases with their corresponding five-color palettes.

### 3.2 Evaluation Metrics

The metrics typically used to assess colorization quality are either subjective or commonly used mathematical metrics such as PSNR and SSIM [90]. Subjective evaluation is the gold standard for many applications where humans determine the accuracy of the output of the algorithms.

In colorization, although subjective evaluation is used to some extent, it has two limitations: 1) scaling is exceptionally challenging, 2) accurately determining the color is also very difficult. On the other hand, the mathematical metrics are general and may not provide an accurate performance of the algorithms. We provide more insights into the metrics for colorization in the “Future Directions” section.

## 4 COMPARISONS

**Qualitative Comparisons:** The networks mentioned in section 2 are evaluated on the peak signal-to-noise ratio (PSNR), the structural similarity index (SSIM) [90], patch-based contrast quality index (PCQI), and underwater image quality measure (UIQM) measures. Table 1 presents the results for each category for all measures. Real-Time colorization [34] achieves high performance of **21.93 dB** and **0.881** for PSNR and SSIM against other competitive measures. Furthermore, the PCQI performance of Instance-Aware colorization [83] and IQM achievement of Colorful colorization [18] are higher compared to state-of-the-art methods. However, declaring one method against the other may not be a simple task due to the involvement of many various elements such as the number of parameters, depth of the network, the number of images for training, the datasets employed, the size of the training patch, the number of feature maps and the network complexity *etc.*. For a fair comparison, the only possible approach is to ensure that all methods have similar elements, as mentioned earlier.

**Quantitative Comparisons:** We present the visual colorization comparisons on fruits and vegetables in Figure 10 and 11, respectively, for few state-of-the-art algorithms. We can observe that most of the algorithms fail to recover the

original natural colors for most of the images. Though Real-Time [34] and Instance-Aware [83] colorization algorithms provide consistent performance and colors closer to the original objects; however, the algorithms are still far from delivering accurate colorization performance. The experiments on the proposed Natural-Color Dataset (NCD) shows the limitation of the state-of-the-art algorithms and encourages the authors to explore novel colorization techniques.

## 5 LIMITATIONS AND FUTURE DIRECTIONS

**Lack of Appropriate Evaluation Metrics:** As mentioned earlier, colorization papers typically employ metrics from image restoration tasks, which may not be appropriate for the task at hand. We also propose that instead of comparing YUV, only the predicted color channels *i.e.* U-channel and V-Channel should be compared. Similarly, it will be highly sought after to use metrics specifically designed to take color into account, such as PCQI [91] and UIQM [92].

PCQI stands for Patch-based contrast quality index. It is a patch-based evaluation metric. It considers three statistics of a patch *i.e.* mean intensity ( $p_m$ ), signal strength or contrast change ( $p_c$ ), and structure distortion ( $p_s$ ) for comparison with ground-truth. It can be expressed as

$$PCQI = p_m(x, y) \cdot p_c(x, y) \cdot p_s(x, y). \quad (3)$$

Similarly, UIQM is the abbreviation of underwater image quality measure. It is different from earlier defined evaluation metrics as it does not require a reference image. Like PCQI, it also depends on three measures *i.e.* image colorfulness, image sharpness, and image contrast. It can be formulated as:

$$IQM = w_1(ICM) + w_2(ISM) + w_3(IConM), \quad (4)$$

where ICM, ISM, and IConM stand for image colorfulness, image sharpness and image contrast, respectively while “ $w$ ” controls the weight of each quantity.

**Lack of Benchmark Dataset:** Image colorization techniques are typically evaluated on grayscale images from various datasets available in the literature due to the absence of purposefully built colorization datasets. The available datasets were originally collected for tasks such as detection, classification, *etc.* contrary to the image colorization. The quality of the images may not be sufficient for image colorization.

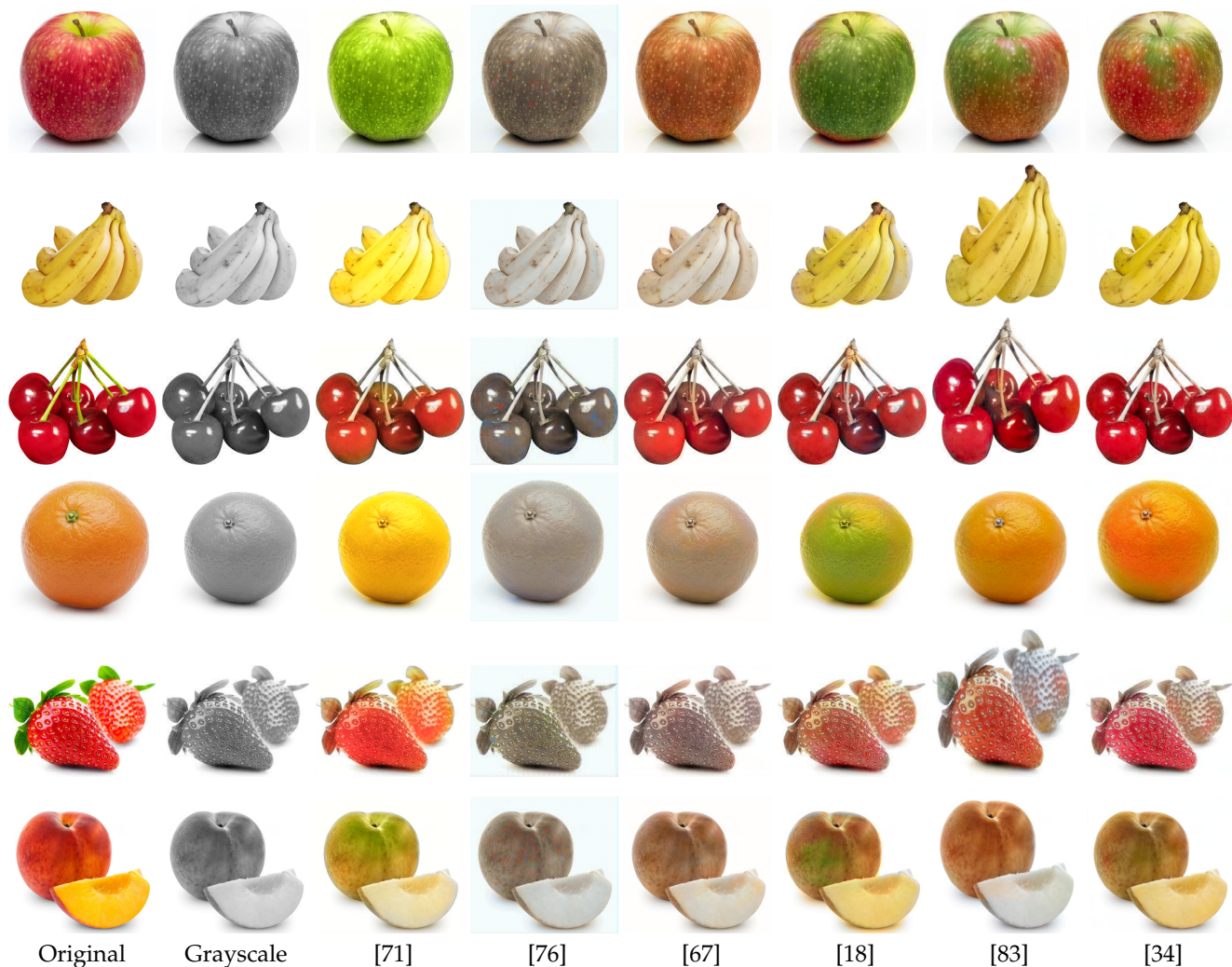


Fig. 10. Visual comparison of colorization algorithms on different fruit images from the Natural-Color Dataset. State-of-the-art colorization algorithms are unable to colorize the images effectively.

Moreover, the datasets contain objects, such as buses, shirts, doors, *etc.*, that can take any color. Hence such an evaluation environment is not appropriate for fair comparison in terms of PSNR or SSIM. We aim to remove this unrealistic setting for image colorization by collecting images that are true to their colors. For example, a carrot will have an orange color in most images. Bananas will be either greenish or yellowish. We have collected 723 images from the internet distributed in 20 categories. Each image has an object and a white background. Our benchmark outlines a realistic evaluation scenario that differs sharply from those generally employed by the image colorization techniques. Figure 9 shows the images from each category from our Natural-Color Dataset (NCD).

**Lacking of Competitions:** Currently, most vision tasks have competitions held across different top-tier conferences *e.g.* (CVPR, ECCV workshops such as NTIRE, PBVS, *etc.*) and online submission platforms, such as Kaggle. These competitions help push state-of-the-art. Unfortunately, there is no such arrangement for image colorization. Making competitions a regular feature in top-tier conferences and online venues would thus be a drastic step forward for image

colorization.

**Limited Availability of Open-Source Codes:** Open-source code plays a vital role in the advancement of the research fields, as can be seen in classification [28], image super-resolution [93], image denoising [94] *etc.* In image colorization, open-source codes are rare or codes are obsolete now as they were built in earlier CNN frameworks. In other fields of research, the codes are either recycled or re-implemented by volunteers in the corresponding field to the new frameworks and environments. However, this is not currently being done for image colorization, hindering progress.

## 6 CONCLUSION

Single-image colorization is a research problem with critical real-life applications. Deep learning approaches' exceptional success has resulted in rapid growth in deep convolutional techniques for image colorization. Based on exciting innovations, various methods are proposed exploiting network structures, training methods, and learning paradigms *etc.* This article presents a thorough review of deep learning methods for image colorization.

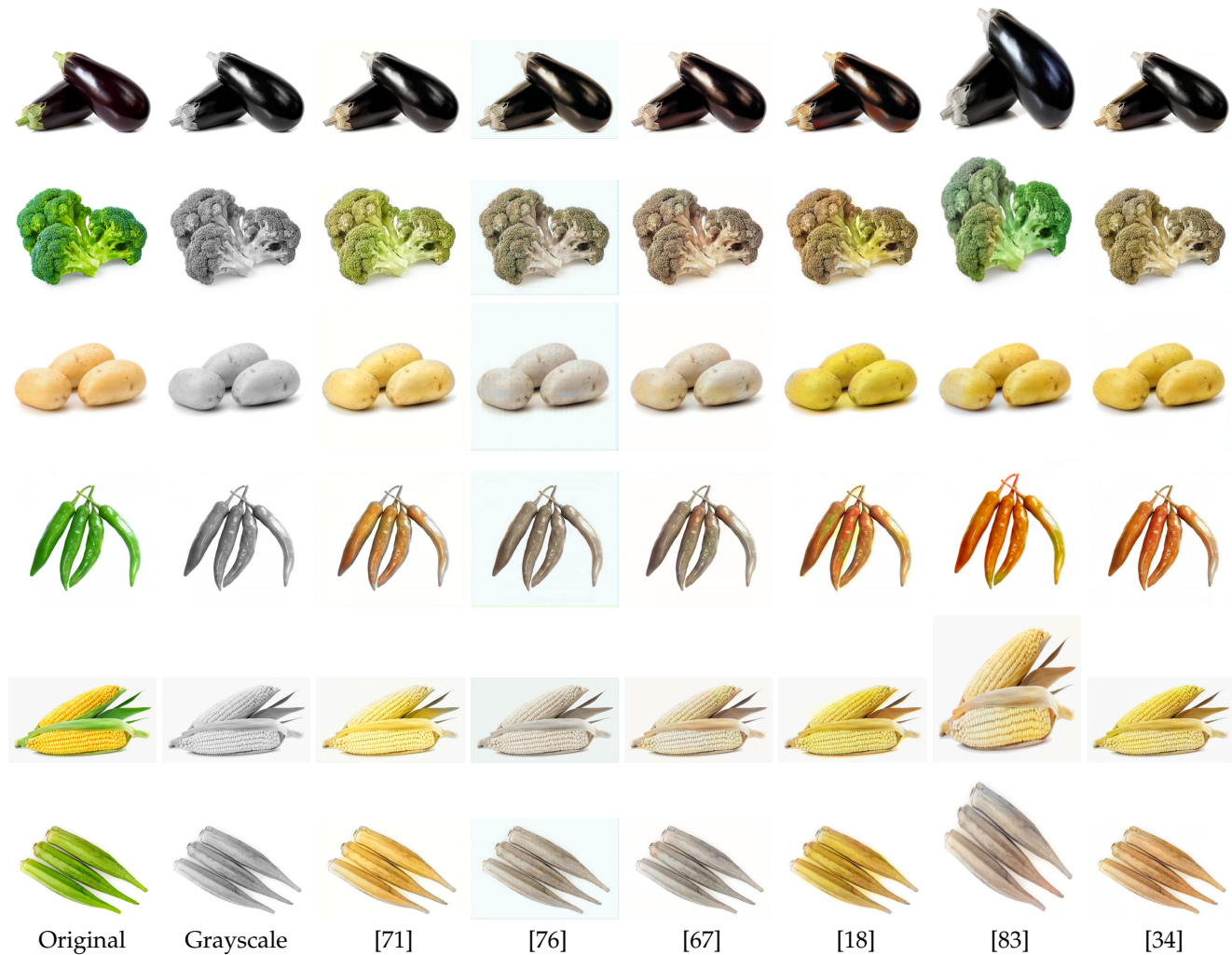


Fig. 11. Qualitative comparison on a few sample images of vegetables from Natural-Color Dataset. Most of the algorithms fail to reproduce the original colors.

We observe image colorization performance has improved in recent years at the cost of increasing the network complexity. However, state-of-the-art methods application to critical real-world scenarios is restricted due to inadequate metrics, network complexity, and failure to handle real-life degradations.

We observe the following trends in image colorization. 1) GAN-based methods deliver diverse colorization visually compared to CNN-based methods, 2) the existing models generally deliver a sub-optimal result for complex scenes having a large number of objects with small sizes, 3) deep models with higher complexity have little improvement in terms of numbers, 4) the diversity of networks in image colorization as compared to other image restoration is significant, 5) a future direction for image colorization is unsupervised learning, 6) many recent advancements and techniques such as attention mechanism, and loss functions can be incorporated for performance. We believe this article and novel dataset will attract further attempts to resolve the mentioned crucial problems.

## REFERENCES

- [1] Z. Cheng, Q. Yang, and B. Sheng, "Deep colorization," in *IEEE International Conference on Computer Vision*, 2015, pp. 415–423.
- [2] S. Yoo, H. Bahng, S. Chung, J. Lee, J. Chang, and J. Choo, "Coloring with limited data: Few-shot colorization via memory augmented networks," in *IEEE Conference on Computer Vision and Pattern Recognition*, 2019, pp. 11 283–11 292.
- [3] T. Welsh, M. Ashikhmin, and K. Mueller, "Transferring color to greyscale images," in *29th annual conference on Computer graphics and interactive techniques*, 2002, pp. 277–280.
- [4] A. Levin, D. Lischinski, and Y. Weiss, "Colorization using optimization," in *Proceedings of International Conference on Computer Graphics and Interactive Techniques' ACM*, 2004, pp. 689–694.
- [5] Y.-C. Huang, Y.-S. Tung, J.-C. Chen, S.-W. Wang, and J.-L. Wu, "An adaptive edge detection based colorization algorithm and its applications," in *13th annual ACM international conference on Multimedia*, 2005, pp. 351–354.
- [6] Y. Qu, T.-T. Wong, and P.-A. Heng, "Manga colorization," *ACM Transactions on Graphics (TOG)*, vol. 25, no. 3, pp. 1214–1220, 2006.
- [7] L. Yatziv and G. Sapiro, "Fast image and video colorization using chrominance blending," *IEEE transactions on image processing*, vol. 15, no. 5, pp. 1120–1129, 2006.
- [8] Q. Luan, F. Wen, D. Cohen-Or, L. Liang, Y.-Q. Xu, and H.-Y. Shum, "Natural image colorization," in *18th Eurographics conference on Rendering Techniques*, 2007, pp. 309–320.
- [9] T. Pärnamaa and L. Parts, "Accurate classification of protein subcellular localization from high-throughput microscopy images

TABLE 1

Comparisons of the state-of-the-art methods for the colorization in terms of PSNR, SSIM, PCQI, and IQM on our Natural-Color Dataset. The higher value of the metrics indicates better performance.

Category	No. of Images	Automatic Colorizer [71]				ColorCapsNet [76]				Let there be Color [67]				Colorful Colorization [18]				Instance-Aware Colorization [83]				Real-Time Colorization [34]			
		PSNR	SSIM	PCQI	IQM	PSNR	SSIM	PCQI	IQM	PSNR	SSIM	PCQI	IQM	PSNR	SSIM	PCQI	IQM	PSNR	SSIM	PCQI	IQM	PSNR	SSIM	PCQI	IQM
Apple	39	16.66	0.772	0.881	1.009	17.64	0.625	0.825	0.869	20.17	0.820	0.918	0.944	18.71	0.792	0.922	1.095	21.94	0.903	0.918	0.918	21.27	0.888	0.915	1.104
Banana	44	17.83	0.792	0.937	0.688	16.43	0.598	0.820	0.652	16.74	0.733	0.936	0.634	22.22	0.894	0.948	0.813	22.14	0.889	0.947	0.643	23.34	0.923	0.948	0.780
Brinjal	35	27.21	0.849	0.946	1.179	26.32	0.720	0.876	1.015	27.74	0.866	0.939	1.094	24.52	0.829	0.946	1.304	25.59	0.843	0.949	1.134	27.56	0.855	0.944	1.242
Broccoli	35	18.57	0.870	0.895	1.419	18.48	0.717	0.865	1.232	18.59	0.816	0.918	1.301	19.34	0.842	0.920	1.483	20.11	0.851	0.942	1.431	19.54	0.854	0.918	1.435
Capsicum green	35	18.72	0.812	0.894	1.097	19.67	0.646	0.840	0.918	19.35	0.731	0.914	0.970	19.91	0.807	0.917	1.168	18.02	0.752	0.927	1.140	19.32	0.789	0.910	1.118
Carrot	39	23.10	0.929	0.931	0.921	17.65	0.655	0.852	0.748	19.40	0.826	0.927	0.825	21.16	0.917	0.939	1.026	22.00	0.908	0.932	0.832	22.62	0.937	0.936	1.005
Cherry	34	23.09	0.892	0.920	1.055	19.71	0.656	0.839	0.927	22.74	0.868	0.919	0.993	23.93	0.896	0.918	1.197	23.47	0.891	0.919	1.042	24.28	0.902	0.924	1.169
Chilli green	36	20.82	0.868	0.944	1.115	20.77	0.716	0.889	0.882	20.86	0.844	0.944	0.962	20.94	0.872	0.948	1.224	20.38	0.858	0.963	1.193	21.39	0.878	0.946	1.154
Corn	36	19.41	0.873	0.911	1.079	15.34	0.584	0.820	0.925	17.03	0.780	0.903	0.997	20.25	0.888	0.905	1.163	19.15	0.849	0.912	1.035	20.44	0.910	0.902	1.146
Cucumber	35	22.58	0.879	0.919	1.304	22.73	0.725	0.862	1.059	22.70	0.834	0.927	1.157	21.63	0.837	0.931	1.409	21.34	0.817	0.955	1.310	23.24	0.865	0.929	1.321
Lady Finger	36	20.66	0.874	0.925	1.189	21.42	0.721	0.876	0.878	21.69	0.848	0.926	0.990	21.64	0.882	0.928	1.246	21.50	0.866	0.954	1.110	23.04	0.903	0.926	1.148
Lemon	39	19.15	0.877	0.873	0.899	14.47	0.551	0.766	0.786	15.37	0.697	0.873	0.816	20.43	0.878	0.875	0.978	21.13	0.894	0.895	0.841	21.20	0.901	0.876	0.962
Orange	29	19.27	0.905	0.873	0.896	13.98	0.536	0.784	0.793	15.16	0.696	0.894	0.788	19.49	0.895	0.899	0.989	21.44	0.915	0.895	0.816	21.06	0.909	0.898	0.991
Peach	27	17.99	0.841	0.849	0.882	16.09	0.550	0.789	0.820	18.63	0.797	0.876	0.811	19.07	0.857	0.902	1.010	19.39	0.833	0.878	0.739	19.53	0.861	0.901	0.997
Pear	28	19.60	0.883	0.926	0.985	16.72	0.591	0.835	0.831	18.59	0.796	0.932	0.888	23.13	0.917	0.943	1.057	21.14	0.893	0.952	0.915	23.87	0.935	0.940	1.026
Plant	35	21.48	0.726	0.888	1.212	22.14	0.626	0.836	1.063	23.43	0.768	0.898	1.114	21.87	0.747	0.901	1.310	20.59	0.734	0.912	1.195	23.37	0.764	0.901	1.263
Pomegranate	55	19.47	0.875	0.901	1.285	16.44	0.602	0.843	1.112	17.56	0.740	0.915	1.165	19.25	0.853	0.925	1.338	19.92	0.863	0.949	1.240	18.72	0.817	0.922	1.295
Potato	35	24.48	0.939	0.862	1.028	18.83	0.622	0.766	0.869	21.81	0.854	0.962	0.945	22.43	0.935	0.860	1.102	23.53	0.935	0.892	1.022	23.19	0.946	0.857	1.046
Strawberry	35	20.84	0.920	0.955	1.444	15.48	0.621	0.880	1.157	15.96	0.743	0.932	1.222	19.13	0.881	0.932	1.485	19.59	0.891	0.972	1.440	20.24	0.898	0.920	1.466
Tomato	48	18.66	0.883	0.933	1.443	15.43	0.584	0.819	0.815	17.44	0.777	0.918	0.858	19.49	0.876	0.918	1.043	20.04	0.878	0.924	0.901	21.30	0.895	0.913	1.036
<b>Dataset-level</b>	<b>735</b>	<b>20.48</b>	<b>0.863</b>	<b>0.906</b>	<b>1.082</b>	<b>18.29</b>	<b>0.632</b>	<b>0.834</b>	<b>0.917</b>	<b>19.55</b>	<b>0.792</b>	<b>0.914</b>	<b>0.974</b>	<b>20.93</b>	<b>0.865</b>	<b>0.919</b>	<b>1.172</b>	<b>21.12</b>	<b>0.863</b>	<b>0.931</b>	<b>1.045</b>	<b>21.93</b>	<b>0.881</b>	<b>0.916</b>	<b>1.135</b>

using deep learning," *G3: Genes, Genomes, Genetics*, vol. 7, no. 5, pp. 1385–1392, 2017.

- [10] M. Xiao, X. Shen, and W. Pan, "Application of deep convolutional neural networks in classification of protein subcellular localization with microscopy images," *Genetic epidemiology*, 2019.
- [11] T. Young, D. Hazarika, S. Poria, and E. Cambria, "Recent trends in deep learning based natural language processing [review article]," *IEEE Computational Intelligence Magazine*, vol. 13, no. 3, pp. 55–75, 2018.
- [12] Z. Zhao, P. Zheng, S. Xu, and X. Wu, "Object detection with deep learning: A review," *IEEE Transactions on Neural Networks and Learning Systems*, vol. 30, no. 11, pp. 3212–3232, 2019.
- [13] S. Anwar, S. Khan, and N. Barnes, "A deep journey into super-resolution: A survey," *ACM Comput. Surv.*, vol. 53, no. 3, May 2020. [Online]. Available: <https://doi.org/10.1145/3390462>
- [14] N. Aafaq, A. Mian, W. Liu, S. Z. Gilani, and M. Shah, "Video description: A survey of methods, datasets, and evaluation metrics," *ACM Comput. Surv.*, vol. 52, no. 6, Oct. 2019. [Online]. Available: <https://doi.org/10.1145/3355390>
- [15] G. Petschnigg, R. Szeliski, M. Agrawala, M. Cohen, H. Hoppe, and K. Toyama, "Digital photography with flash and no-flash image pairs," *ACM transactions on graphics (TOG)*, vol. 23, no. 3, pp. 664–672, 2004.
- [16] E. Tola, V. Lepetit, and P. Fua, "A fast local descriptor for dense matching," in *2008 IEEE conference on computer vision and pattern recognition*, 2008, pp. 1–8.
- [17] F. M. Carlucci, P. Russo, and B. Caputo, "(DE)<sup>2</sup> CO: Deep depth colorization," *IEEE Robotics and Automation Letters*, vol. 3, no. 3, pp. 2386–2393, 2018.
- [18] R. Zhang, P. Isola, and A. A. Efros, "Colorful image colorization," in *European conference on computer vision*. Springer, 2016, pp. 649–666.
- [19] J. Xiao, J. Hays, K. A. Ehinger, A. Oliva, and A. Torralba, "Sun database: Large-scale scene recognition from abbey to zoo," in *2010 IEEE Computer Society Conference on Computer Vision and Pattern Recognition*, 2010, pp. 3485–3492.
- [20] S. Ioffe and C. Szegedy, "Batch normalization: Accelerating deep network training by reducing internal covariate shift," in *International Conference on Machine Learning*, 2015, pp. 448–456.
- [21] Y. Jia, E. Shelhamer, J. Donahue, S. Karayev, J. Long, R. Girshick, S. Guadarrama, and T. Darrell, "Caffe: Convolutional architecture for fast feature embedding," in *22nd ACM international conference on Multimedia*, 2014, pp. 675–678.
- [22] D. P. Kingma and J. Ba, "Adam: A method for stochastic optimization," *International Conference on Learning Representations*, 2015.
- [23] J. Deng, W. Dong, R. Socher, L.-J. Li, K. Li, and L. Fei-Fei, "Imagenet: A large-scale hierarchical image database," in *IEEE conference on computer vision and pattern recognition*, 2009, pp. 248–255.
- [24] A. L. Maas, A. Y. Hannun, and A. Y. Ng, "Rectifier nonlinearities improve neural network acoustic models," in *Proc. icml*, vol. 30, no. 1, 2013, p. 3.
- [25] A. Krizhevsky, I. Sutskever, and G. E. Hinton, "Imagenet classification with deep convolutional neural networks," in *Advances in neural information processing systems*, 2012, pp. 1097–1105.
- [26] K. Simonyan and A. Zisserman, "Very deep convolutional networks for large-scale image recognition," *International Conference on Learning Representations*, 2015.
- [27] C. Szegedy, Wei Liu, Yangqing Jia, P. Sermanet, S. Reed, D. Anguelov, D. Erhan, V. Vanhoucke, and A. Rabinovich, "Going deeper with convolutions," in *2015 IEEE Conference on Computer Vision and Pattern Recognition (CVPR)*, 2015, pp. 1–9.
- [28] K. He, X. Zhang, S. Ren, and J. Sun, "Deep residual learning for image recognition," in *IEEE conference on computer vision and pattern recognition*, 2016, pp. 770–778.
- [29] K. Lai, L. Bo, X. Ren, and D. Fox, "A large-scale hierarchical multi-view rgb-d object dataset," in *2011 IEEE international conference on robotics and automation*, 2011, pp. 1817–1824.
- [30] C. Li, A. Reiter, and G. D. Hager, "Beyond spatial pooling: fine-grained representation learning in multiple domains," in *IEEE Conference on Computer Vision and Pattern Recognition*, 2015, pp. 4913–4922.
- [31] A. Singh, J. Sha, K. S. Narayan, T. Achim, and P. Abbeel, "Big-bird: A large-scale 3d database of object instances," in *2014 IEEE international conference on robotics and automation (ICRA)*, 2014, pp. 509–516.
- [32] P. Sangkloy, J. Lu, C. Fang, F. Yu, and J. Hays, "Scribbler: Controlling deep image synthesis with sketch and color," in *IEEE Conference on Computer Vision and Pattern Recognition*, 2017, pp. 5400–5409.
- [33] Y. Güçlütürk, U. Güçlü, R. van Lier, and M. A. van Gerven, "Convolutional sketch inversion," in *European Conference on Computer Vision*. Springer, 2016, pp. 810–824.
- [34] R. Zhang, J.-Y. Zhu, P. Isola, X. Geng, A. S. Lin, T. Yu, and A. A. Efros, "Real-time user-guided image colorization with learned deep priors," *ACM Transactions on Graphics (TOG)*, vol. 36, no. 4, pp. 1–11, 2017.
- [35] Y. Xiao, P. Zhou, Y. Zheng, and C.-S. Leung, "Interactive deep colorization using simultaneous global and local inputs," in *ICASSP 2019 - 2019 IEEE International Conference on Acoustics, Speech and Signal Processing (ICASSP)*, 2019, pp. 1887–1891.
- [36] Y. Ci, X. Ma, Z. Wang, H. Li, and Z. Luo, "User-guided deep anime line art colorization with conditional adversarial networks," in *26th ACM international conference on Multimedia*, 2018, pp. 1536–1544.
- [37] O. Ronneberger, P. Fischer, and T. Brox, "U-net: Convolutional networks for biomedical image segmentation," in *International Conference on Medical image computing and computer-assisted intervention*. Springer, 2015, pp. 234–241.
- [38] B. Zhou, A. Lapedriza, A. Torralba, and A. Oliva, "Places: An image database for deep scene understanding," *Journal of Vision*, vol. 17, no. 10, pp. 296–296, 2017.
- [39] M. Mirza and S. Osindero, "Conditional generative adversarial nets," in *Advances in Neural Information Processing Systems*, p. s 2672–2680, 2014.
- [40] M. Saito and Y. Matsui, "Illustration2vec: a semantic vector representation of illustrations," in *SIGGRAPH Asia 2015 Technical Briefs*, 2015, pp. 1–4.
- [41] S. Xie, R. Girshick, P. Dollár, Z. Tu, and K. He, "Aggregated residual transformations for deep neural networks," in *IEEE conference on computer vision and pattern recognition*, 2017, pp. 1492–1500.

- [42] C. Ledig, L. Theis, F. Huszár, J. Caballero, A. Cunningham, A. Acosta, A. Aitken, A. Tejani, J. Totz, Z. Wang *et al.*, “Photo-realistic single image super-resolution using a generative adversarial network,” in *IEEE conference on computer vision and pattern recognition*, 2017, pp. 4681–4690.
- [43] M. Limmer and H. P. Lensch, “Infrared colorization using deep convolutional neural networks,” in *2016 15th IEEE International Conference on Machine Learning and Applications (ICMLA)*, 2016, pp. 61–68.
- [44] L. Junsoo, K. Eungyeup, L. Yunsung, K. Dongjun, C. Jaehyuk, and C. Jaegul, “Reference-based sketch image colorization using augmented-self reference and dense semantic correspondence,” in *IEEE conference on computer vision and pattern recognition*, 2020, pp. 5801–5810.
- [45] Q. Song, F. Xu, and Y.-Q. Jin, “Radar image colorization: Converting single-polarization to fully polarimetric using deep neural networks,” *IEEE Access*, vol. 6, pp. 1647–1661, 2017.
- [46] P. Wang and V. M. Patel, “Generating high quality visible images from sar images using cnns,” in *2018 IEEE Radar Conference (Radar-Conf18)*, 2018, pp. 0570–0575.
- [47] V. Manjunatha, M. Iyyer, J. Boyd-Graber, and L. Davis, “Learning to color from language,” in *2018 Conference of the North American Chapter of the Association for Computational Linguistics: Human Language Technologies, Volume 2 (Short Papers)*, 2018, pp. 764–769.
- [48] S. E. Reed, Z. Akata, S. Mohan, S. Tenka, B. Schiele, and H. Lee, “Learning what and where to draw,” in *Advances in neural information processing systems*, 2016, pp. 217–225.
- [49] E. Perez, F. Strub, H. De Vries, V. Dumoulin, and A. Courville, “Film: Visual reasoning with a general conditioning layer,” in *Thirty-Second AAAI Conference on Artificial Intelligence*, 2018.
- [50] T.-Y. Lin, M. Maire, S. Belongie, J. Hays, P. Perona, D. Ramanan, P. Dollár, and C. L. Zitnick, “Microsoft coco: Common objects in context,” in *European conference on computer vision*. Springer, 2014, pp. 740–755.
- [51] H. Bahng, S. Yoo, W. Cho, D. Keetae Park, Z. Wu, X. Ma, and J. Choo, “Coloring with words: Guiding image colorization through text-based palette generation,” in *IEEE European Conference on Computer Vision (ECCV)*, 2018, pp. 431–447.
- [52] A. Radford, L. Metz, and S. Chintala, “Unsupervised representation learning with deep convolutional generative adversarial networks,” in *Proc. the International Conference on Learning Representations (ICLR)*, 2015.
- [53] Y. Cao, Z. Zhou, W. Zhang, and Y. Yu, “Unsupervised diverse colorization via generative adversarial networks,” in *Joint European Conference on Machine Learning and Knowledge Discovery in Databases*. Springer, 2017, pp. 151–166.
- [54] F. Yu, A. Seff, Y. Zhang, S. Song, T. Funkhouser, and J. Xiao, “Lsun: Construction of a large-scale image dataset using deep learning with humans in the loop,” *arXiv preprint arXiv:1506.03365*, 2015.
- [55] K. Frans, “Outline colorization through tandem adversarial networks,” *arXiv preprint arXiv:1704.08834*, 2017.
- [56] K. Nazeri, E. Ng, and M. Ebrahimi, “Image colorization using generative adversarial networks,” in *International Conference on Articulated Motion and Deformable Objects*. Springer, 2018, pp. 85–94.
- [57] A. Deshpande, J. Lu, M.-C. Yeh, M. Jin Chong, and D. Forsyth, “Learning diverse image colorization,” in *IEEE Conference on Computer Vision and Pattern Recognition*, 2017, pp. 6837–6845.
- [58] P. Vitoria, L. Raad, and C. Ballester, “ChromaGAN: Adversarial picture colorization with semantic class distribution,” in *The IEEE Winter Conference on Applications of Computer Vision*, 2020, pp. 2445–2454.
- [59] J. Long, E. Shelhamer, and T. Darrell, “Fully convolutional networks for semantic segmentation,” in *IEEE conference on computer vision and pattern recognition*, 2015, pp. 3431–3440.
- [60] K. He, X. Zhang, S. Ren, and J. Sun, “Delving deep into rectifiers: Surpassing human-level performance on imagenet classification,” in *IEEE international conference on computer vision*, 2015, pp. 1026–1034.
- [61] A. Krizhevsky, G. Hinton *et al.*, “Learning multiple layers of features from tiny images,” *Master’s thesis, University of Tront*, 2009.
- [62] B. Zhou, A. Lapedriza, A. Torralba, and A. Oliva, “Places: An image database for deep scene understanding,” *Journal of Vision*, vol. 17, no. 10, pp. 296–296, 2017.
- [63] P. Isola, J.-Y. Zhu, T. Zhou, and A. A. Efros, “Image-to-image translation with conditional adversarial networks,” in *IEEE conference on computer vision and pattern recognition*, 2017, pp. 1125–1134.
- [64] L. Kaiser, O. Nachum, A. Roy, and S. Bengio, “Learning to remember rare events,” *International Conference on Learning Representations*, 2017.
- [65] M.-E. Nilsback and A. Zisserman, “Automated flower classification over a large number of classes,” in *2008 Sixth Indian Conference on Computer Vision, Graphics & Image Processing*, 2008, pp. 722–729.
- [66] P. Docter, J. Culton, J. Pidgeon, and R. Eggleston, “Monsters, inc.” Walt Disney Pictures, 2001.
- [67] S. Iizuka, E. Simo-Serra, and H. Ishikawa, “Let there be color! joint end-to-end learning of global and local image priors for automatic image colorization with simultaneous classification,” *ACM Transactions on Graphics (ToG)*, vol. 35, no. 4, pp. 1–11, 2016.
- [68] M. D. Zeiler, “Adadelta: an adaptive learning rate method,” *arXiv preprint arXiv:1212.5701*, 2012.
- [69] L. Bottou, “Stochastic gradient learning in neural networks,” *Proceedings of Neuro-Nimes*, vol. 91, no. 8, p. 12, 1991.
- [70] R. Collobert, K. Kavukcuoglu, and C. Farabet, “Torch7: A matlab-like environment for machine learning,” in *BigLearn, NIPS workshop*, no. CONF, 2011.
- [71] G. Larsson, M. Maire, and G. Shakhnarovich, “Learning representations for automatic colorization,” in *European Conference on Computer Vision*. Springer, 2016, pp. 577–593.
- [72] S. Guadarrama, R. Dahl, D. Bieber, M. Norouzi, J. Shlens, and K. Murphy, “Pixcolor: Pixel recursive colorization,” *28th British Machine Vision Conference (BMVC)*, 2017.
- [73] M. H. Baig and L. Torresani, “Multiple hypothesis colorization and its application to image compression,” *Computer Vision and Image Understanding*, vol. 164, pp. 111–123, 2017.
- [74] J. Zhao, J. Han, L. Shao, and C. G. Snoek, “Pixelated semantic colorization,” *International Journal of Computer Vision*, pp. 1–17, 2019.
- [75] J. Zhao, L. Liu, C. Snoek, J. Han, and L. Shao, “Pixel-level semantics guided image colorization,” in *British Machine Vision Conference 2018, BMVC 2018, Northumbria University, Newcastle, UK, September 3-6, 2018*. BMVA Press, 2018, p. 156. [Online]. Available: <http://bmvc2018.org/contents/papers/0236.pdf>
- [76] G. Ozbulak, “Image colorization by capsule networks,” in *IEEE Conference on Computer Vision and Pattern Recognition Workshops*, 2019, pp. 0–0.
- [77] S. Sabour, N. Frosst, and G. E. Hinton, “Dynamic routing between capsules,” in *Advances in neural information processing systems*, 2017, pp. 3856–3866.
- [78] E. Agustsson and R. Timofte, “Ntire 2017 challenge on single image super-resolution: Dataset and study,” in *IEEE Conference on Computer Vision and Pattern Recognition Workshops*, 2017, pp. 126–135.
- [79] M. Everingham, L. Van Gool, C. K. Williams, J. Winn, and A. Zisserman, “The pascal visual object classes (voc) challenge,” *International journal of computer vision*, vol. 88, no. 2, pp. 303–338, 2010.
- [80] M. He, D. Chen, J. Liao, P. V. Sander, and L. Yuan, “Deep exemplar-based colorization,” *ACM Transactions on Graphics (TOG)*, vol. 37, no. 4, p. 47, 2018.
- [81] J. Liao, Y. Yao, L. Yuan, G. Hua, and S. B. Kang, “Visual attribute transfer through deep image analogy,” *ACM Transactions on Graphics (TOG)*, vol. 36, no. 4, pp. 1–15, 2017.
- [82] X. Zhongyou, W. Tingting, F. Faming, S. Yun, and Z. Guixu, “Stylization-based architecture for fast deep exemplar colorization,” in *IEEE conference on computer vision and pattern recognition*, 2020, pp. 9363–9372.
- [83] S. Jheng-Wei, C. Hung-Kuo, and H. Jia-Bin, “Reference-based sketch image colorization using augmented-self reference and dense semantic correspondence,” in *IEEE conference on computer vision and pattern recognition*, 2020, pp. 7968–7977.
- [84] H. Xun and B. Serge, “Arbitrary style transfer in real-time with adaptive instance normalization,” in *ICCV*, 2017, pp. 1501–1510.
- [85] H. Peter, “Robust estimation of a location parameter,” in *Breakthroughs in statistics*, 1992, pp. 492–518.
- [86] H. Caesar, J. Uijlings, and V. Ferrari, “Coco-stuff: Thing and stuff classes in context,” in *IEEE Conference on Computer Vision and Pattern Recognition*, 2018, pp. 1209–1218.
- [87] Z. Bolei, L. Agata, X. Jianxiang, T. Antonio, and O. Aude, “Learning deep features for scene recognition using places dataset,” in *Advances in neural information processing systems*, 2014, pp. 487–495.
- [88] M. Everingham, S. A. Eslami, L. Van Gool, C. K. Williams, J. Winn, and A. Zisserman, “The pascal visual object classes challenge:

- A retrospective," *International journal of computer vision*, vol. 111, no. 1, pp. 98–136, 2015.
- [89] A. Torralba, R. Fergus, and W. T. Freeman, "80 million tiny images: A large data set for nonparametric object and scene recognition," *IEEE transactions on pattern analysis and machine intelligence*, vol. 30, no. 11, pp. 1958–1970, 2008.
- [90] Z. Wang, A. C. Bovik, H. R. Sheikh, and E. P. Simoncelli, "Image quality assessment: from error visibility to structural similarity," *IEEE transactions on image processing*, 2004.
- [91] S. Wang, K. Ma, H. Yeganeh, Z. Wang, and W. Lin, "A patch-structure representation method for quality assessment of contrast changed images," *IEEE Signal Processing Letters*, vol. 22, no. 12, pp. 2387–2390, 2015.
- [92] K. Panetta, C. Gao, and S. Aghaian, "Human-visual-system-inspired underwater image quality measures," *IEEE Journal of Oceanic Engineering*, vol. 41, no. 3, pp. 541–551, 2015.
- [93] S. Anwar and N. Barnes, "Densely residual laplacian super-resolution," *IEEE Transactions on Pattern Analysis and Machine Intelligence*, 2020.
- [94] —, "Real image denoising with feature attention," in *IEEE International Conference on Computer Vision*, 2019, pp. 3155–3164.
- [95] G. Larsson, M. Maire, and G. Shakhnarovich, "Colorization as a proxy task for visual understanding," in *IEEE Conference on Computer Vision and Pattern Recognition*, 2017, pp. 6874–6883.
- [96] W. Jang, "Sampling using neural networks for colorizing the grayscale images," *arXiv preprint arXiv:1812.10650*, 2018.
- [97] T.-Y. Lin, M. Maire, S. Belongie, J. Hays, P. Perona, D. Ramanan, P. Dollár, and C. L. Zitnick, "Microsoft coco: Common objects in context," in *European conference on computer vision*. Springer, 2014, pp. 740–755.
- [98] H. Kim, H. Y. Jhoo, E. Park, and S. Yoo, "Tag2pix: Line art colorization using text tag with secat and changing loss," in *IEEE International Conference on Computer Vision*, 2019, pp. 9056–9065.